Exclusive Enteral Nutrition Initiates Individual Protective Microbiome Changes to Induce Remission in Pediatric Crohn's Disease

Häcker, Deborah[1,2]; Siebert, Kolja[3]; Smith, Byron J[4+]; Köhler, Nikolai[5]; Riva, Alessandra[1]; Mahapatra, Aritra[6]; Heimes, Helena[1]; Nie, Jiatong[1]; Metwaly, Amira[1]; Hölz, Hannes[3]; Manz, Quirin[7]; De Zen, Federica[3]; Heetmeyer, Jeannine[3]; Socas, Katharina[3]; Le Thi, Giang[3]; Meng, Chen[8]; Kleigrewe, Karin[8]; Pauling, Josch K[5]; Neuhaus, Klaus[6]; List, Markus[7,9]; Pollard, Katherine S[4,10,11]; Schwerd, Tobias[3&+]; Haller, Dirk[1,2,6&+]

[&]Authors contributed equally, [+]Corresponding author

[1] Chair of Nutrition and Immunology, TUM School of Life Sciences, Technische Universität München, Freising, Germany

[2] TUMCREATE, 1 CREATE Way, #10-02 CREATE Tower, Singapore 138602

[3] Department of Pediatrics, Dr. von Hauner Children's Hospital, University Hospital, LMU Munich, Germany.

[4] Gladstone Institutes, San Francisco, CA, USA

[5] LipiTUM, Chair of Experimental Bioinformatics, TUM School of Life Sciences, Technical University of Munich, Freising, Germany

[6] ZIEL Institute for Food & Health, Technische Universität München, Freising, Germany

[7] Data Science in Systems Biology, School of Life Sciences, Technische Universität München, Freising, Germany

[8] Bavarian Center for Biomolecular Mass Spectrometry (BayBioMS), TUM School of Life Sciences, Technische Universität München, Freising, Germany

[9] Munich Data Science Institute (MDSI), Technical University of Munich, Garching, Germany

[10] University of California, San Francisco, CA, USA

[11] Chan Zuckerberg Biohub

Correspondence:
Prof. Dr. Dirk Haller
Technical University of Munich
Chair of Nutrition and Immunology
Gregor-Mendel-Str. 2
85354 Freising, Germany
Email: dirk.haller@tum.de
Phone: + 49 8161-71 2026

Keywords: pediatric Crohn's disease, Exclusive enteral nutrition - EEN, fiber, medium chain fatty acids, *ex vivo* gut chemostat model, FMT, multi-omics data integration, microbiome, metagenomics, bacterial strain dynamics

Exclusive Enteral Nutrition

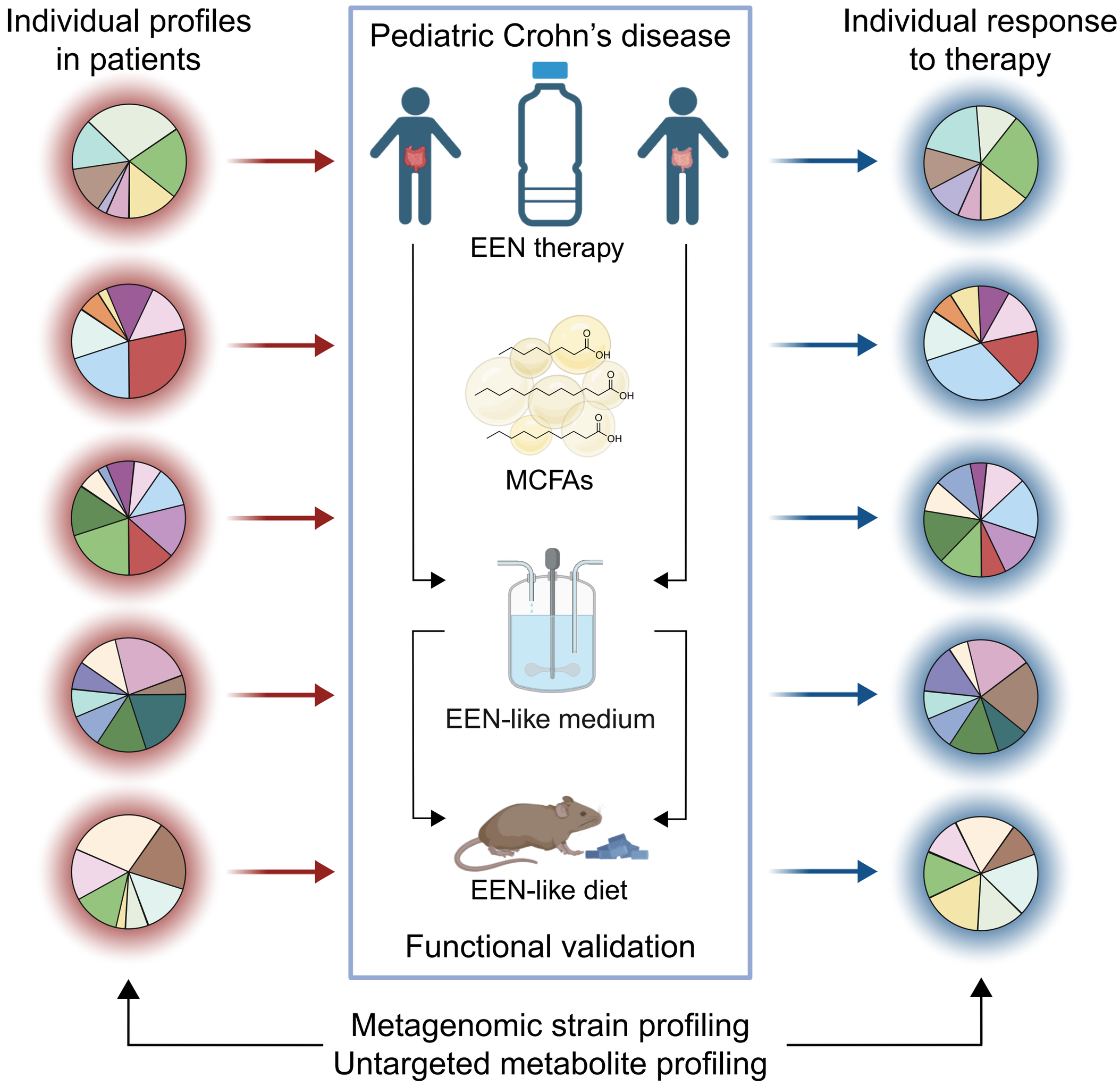

Summary

Exclusive enteral nutrition (EEN) is the first-line therapy for pediatric Crohn's disease (CD), but protective mechanisms remain unknown. We established a prospective pediatric cohort to characterize the function of fecal microbiota and metabolite changes of treatment-naïve CD patients in response to EEN. Integrated multi-omics analysis identified network clusters from individually variable microbiome profiles, with *Lachnospiraceae* and medium chain fatty acids as protective features. Bioorthogonal non-canonical amino acid tagging selectively identified bacterial species in response to medium chain fatty acids. Metagenomic analysis identified high strain-level dynamics in response to EEN. Functional changes of diet-exposed fecal microbiota were further validated in a combined approach using gut chemostat cultures and microbiota transfer into germ-free *Il10*-deficient mice. Dietary model conditions induced individual patient-specific strain signatures to prevent or cause IBD-like inflammation in gnotobiotic mice. Hence, we provide evidence that EEN therapy operates through explicit functional changes of temporally and individually variable microbiome profiles.

Introduction

Crohn's disease (CD), one of the main entities of inflammatory bowel diseases (IBD), is a chronic and relapsing inflammatory condition of the gastrointestinal tract[1]. Epidemiological studies have demonstrated a significant increase in the incidence of CD in Westernized countries, particularly among the pediatric age group[2,3]. The pathogenesis of IBD involves host genetics and environmental influences, among which diet and the intestinal microbiome are key etiologic factors[4,5].

Exclusive enteral nutrition (EEN) is the first-line treatment for pediatric CD[6,7] and also shows efficacy in adult patients[8]. EEN refers to polymeric liquid formulas, which are mostly devoid of fibers[9]. Re-introducing regular diet after 6-8 weeks of EEN often results in recurrence of inflammation and disease activity[10]. EEN has been shown to drive changes in gut microbiota composition[11], but the high relapse rate after cessation of EEN suggests the presence of a CD-conditioned microbiome, which is able to re-establish after dietary intervention[12]. CD is associated with reduced bacterial diversity, compositional and functional changes, and the disruption of metabolic circuits between microbiome and host[13–15]. Despite recent findings that EEN mediates protective functions in experimental models of colitis[16], human studies revealed incomplete recovery of the intestinal microbiome after antibiotic interventions[17]. Thus, functional evidence for EEN-mediated changes in the human microbiome as an underlying cause of therapeutic efficacy is still lacking.

Here, we identify EEN-protective signatures using integrated microbiota and metabolite analysis of treatment-naïve pediatric CD patients. Medium chain fatty acids (MCFAs) directly target bacteria from of the EEN-protective signatures, providing a direct mechanistic link between diet and microbiota changes. Further, we established a combined gut chemostat-to-mouse transfer approach to functionally validate EEN-mediated protective changes in the microbiome of CD patients. We demonstrate that EEN directly shapes microbiomes to mediate protective functions in treatment-naïve CD patients, operating through explicit patient-to-patient changes of temporally and individually variable strain profiles.

Results

Microbiota and metabolite profiling identify individual responses to EEN therapy in pediatric CD patients

We established a pediatric IBD cohort and longitudinally followed 78 IBD patients, showing no disease specific but individual bacterial and metabolite profiles in fecal samples (**Fig. 1A, S1A-C**). To gain insides in mechanisms of EEN therapy, we focused explicitly on 20 newly diagnosed and treatment-naïve CD patients, receiving EEN as induction therapy (CD-EEN group, 9 females, age at study inclusion 12.5 ± 3.1 years) (**Fig. 1A, S1A; Table S1**). EEN was highly effective and significantly improved disease activity and inflammatory markers at the end of EEN treatment, resulting in clinical response and induction of remission in 20/20 and 18/20 patients, respectively (**Fig. 1B**). During follow-up, patients received methotrexate (6/20), anti-TNF (13/20), or combination therapies (9/13) as maintenance treatment. Relapse after EEN was observed in 8/20 patients over one-year follow-up (**Fig. 1B**). Two patients switched from Modulen IBD® to Neocate Junior® during EEN due to suspected cow's milk protein allergy.

Analysis of samples before (PreEEN), during (EEN), and after EEN therapy (PostEEN) (microbiota profiling: 291 samples, metabolomic analysis: 145 samples) revealed patient-specific responses (**Fig. 1C, D**). Bacterial richness based on zOTUs (zero-radius operational taxonomic units) changed individually during formula feeding (**Fig. S1D**) but was lower during active CD compared to remission (**Fig. S1E**). Samples of EEN-treated patients are scattered throughout dendrograms of microbiota and metabolome profiles (**Fig. 1C, D**). Despite considerable overlap in multi-dimensional scaling (MDS) plots based on microbial profiles, linear mixed models (LMMs) identified only diet as significantly contributing to the first MDS dimension (x-axis) (**Fig. 1E**, n=277, p-value < 0.0001; **Fig. S1F**). PCA plots of metabolic profiles also showed significant separation according to diet along PC2 but no separation according to disease activity (**Fig. 1F**, n = 141, p-value < 0.0001; **Fig. S1G**).

107 **Integration of microbiota and metabolome data identifies key features of EEN exposure**

108 To identify key differences between fecal microbiota and metabolite profiles of patients
109 collected under EEN (therapy, partially with still active disease) and PostEEN conditions
110 (receiving regular diets but completely in remission), a network analysis incorporating matched
111 zOTU taxonomic profiles and untargeted metabolomics from 60 samples was performed. The
112 identified interlinked features clustered in five distinct network communities (**Fig. S2**). In
113 summary for the top selected features from the correlation network, higher mean importance
114 was found for zOTUs associated to EEN compared to zOTUs associated with PostEEN (**Fig.**
115 **1I**). The top eleven zOTUs associated to EEN were found within all communities (**Fig. 1I**, green
116 gradient), including several zOTUs from the genera *Enterocloster* and *Clostridium* (formerly
117 *Lachnoclostridium; Lachnospiraceae;* **Table S2**) which still showed individual abundances in
118 each patient (**Fig. S3A**). Of the 22 top selected metabolite features, the majority were
119 associated with PostEEN, whereas six metabolites were associated with EEN with higher
120 mean importance (**Fig. 1J**). Of the in total ten metabolites associated with EEN, the majority
121 of those were medium chain fatty acids (MCFA) (palmitoleic acid, decanoic acid, caprylic acid
122 and lauric acid) which were identified as metabolite features present in Modulen IBD® (**Fig.**
123 **S2C, S3B**).
124

125 **Medium chain fatty acids selectively induce translational activation of fecal bacteria**

126 Three MCFAs [(lauric acid (LA), decanoic (DA) acid and octanoic acid (OA)] were identified as
127 signature metabolites of EEN, likely originating from IBD Modulen. To determine which gut
128 bacteria can be activated by these metabolites, we employed a combination of bioorthogonal
129 noncanonical amino acid tagging (BONCAT) and fluorescence-activated cell sorting (FACS)
130 to identify translationally active bacteria in the presence of MCFAs under *ex vivo* anaerobic
131 incubations (**Fig. 2A**). We selected three donors (MP1-MP3, model patient) within the CD-EEN
132 group based on clinical activity, limited drug exposure and chose four different samples along
133 EEN therapy (**Table S3,** STAR Methods, **Fig. 4A, C, I; S8F**). Confocal microscopy visualization
134 and quantification indicated that a significantly higher proportion of gut bacteria became
135 translationally active after exposure to MCFAs, compared to the solvent control (**Fig. 2B, C;**
136 **Fig. S4, S5**). The MCFA-active fraction of the community (BONCAT labeling and FACS
137 sorting), exhibited significant differences compared to the unsorted community and between
138 patients as shown in the MDS ordination ($p = 0.001$, **Fig. 2D**). Ethanol mediated variability is
139 shown as additional control (**Fig. S5C**). This separation highlights distinct microbial
140 communities to be present after MCFAs exposure. We identified different zOTUs enriched in
141 the active fraction after exposure to MCFAs compared to the ethanol control (**Fig. 2E, S5;**
142 **Table S4, S5**). Different species from the *Enterocloster* genera were significantly enriched in

143 response to MCFAs, especially in MP2 at EEN remission stage (**Fig. 2E**). This includes
144 *Enterocloster aldensis* and two subspecies of *Enterocloster boltae*, which aligns with the
145 bacterial signature identified from the clinical cohort (**Fig. 1G**). Additional enriched taxa
146 included *Eggerthella lenta* in MP2 (remission); *Escherichia coli, Clostridium scindens, Dialister*
147 *invisus, Sporobacter* spp. *and Eubacterium* spp. (MP2 relapse); *E. coli* in MP1 and MP3 as
148 well as *Lachnospiraceae* in MP1. In contrast, several additional zOTUs were depleted in the
149 active fraction after MCFA exposure including *Clostridium scindens, Thomasclavelia ramosa,*
150 *Hungatella hominis, Peptostreptococcus anaerobius, Ruthenibacterium lactatiformans* and
151 *Phocaeicola vulgatus* in MP2 at EEN remission stage and *Anaerostipes hadrus* and
152 *Hominenteromicrobium mulieris* in MP2 under relapse (**Fig. 2E, S5, Table S4, S5**). In
153 summary, of the 16 zOTUs associated with EEN from the Network analyses, 8 zOTUs
154 responded to MCFA exposure (labeled with * in **Fig. 1G, S2C**).

155 **Microbial species, strains, and functions change dramatically at EEN cessation**

156 Considering the various changes of community profiles associated with EEN or PostEEN, we
157 next investigated dynamics within the patients along EEN therapy. Cessation of EEN resulted
158 in an elevated turnover in zOTU composition (**Fig. 3A**), resulting in higher dissimilarity - even
159 after controlling for greater time periods - between pairs of samples spanning the transition off
160 of EEN compared to during or post-EEN alone ($p < 10^{-3}$ for both comparisons by permutation
161 test). Using shotgun metagenomes for 96 CD-EEN patient samples (n = 19 patients), we
162 applied StrainFacts[18] to resolve taxonomic differences below the level of species. Like zOTUs,
163 and despite the much smaller number of comparisons, we detected the same elevated turnover
164 in the composition of strains during the transition off of EEN relative to the PostEEN period (p
165 $< 10^{-3}$, **Fig. 3B**). Overall, we observed high strain-level diversity within and between CD-EEN
166 patients. For most of the 369 species, individual strains were largely specific to a single patient
167 and appeared in multiple samples from their host, while some samples contained multiple
168 distinct strains of a given species (e.g. **Fig. 3D-F**).

169 Besides taxonomic turnover, we also detected 583 protein coding gene families (COGs) with
170 substantial changes in their normalized abundance (54 increased and 529 decreased) at the
171 transition off of EEN (**Fig. 3C**). Families increased during EEN included COG3845 (mean log2
172 PostEEN/EEN of -0.58) and COG4603 (-0.58), components of the ABC-type guanosine uptake
173 system. Increases in COG4813 (+2.1), annotated as trehalose utilization protein, and
174 COG3867 (+1.0), arabinogalactan endo-1,4-beta-galactosidase, indicate that microbes
175 encoding these proteins respond to host diet and may play a role in metabolite transformations.
176 These findings are consistent with changes in carbohydrates and sugar acids found in the
177 metabolite analysis (**Fig. S2C**).

178 Next, we sought to identify species with high prevalence and abundance and with large
179 changes in relative abundance or extensive strain turnover at the end of EEN. Using an
180 indicator score based on these features (**Fig. S2A, Table S7**), we flagged 46 species as highly
181 dynamic. We identified pairs of zOTUs and metagenomic species (**Table S6**) and matched 37
182 (80%) of the top scoring species (**Fig. S6B, Table S7**). Here we highlight and contrast the
183 strain dynamics of two closely related species, *Enterocloster bolteae* (formerly
184 *Lachnoclostridium bolteae*) and *E. clostridioformis* (formerly *C. clostridioforme*). Both of these
185 species were matched to zOTU5 (**Fig. S6C**) and showed dynamic strain composition over
186 patient time series (**Fig. 3D, E**). In some patients, EEN and PostEEN samples contained similar
187 strains of each species, but the dominant strain changed; in others, a new strain appeared
188 PostEEN that was absent or undetectable during EEN. Interestingly, the relative abundance of
189 *E. bolteae*, but not *E. clostridioformis*, was significantly affected by EEN cessation ($p = 0.018$
190 and 0.9, respectively, by Wilcoxin test; **Table S7**). Hower, while both showed a similar strain
191 turnover overall, *E. clostridioformis*, but not *E. bolteae* had significantly elevated strain turnover
192 at the transition from EEN to PostEEN ($p = 0.004$ and 0.202, respective, by permutation test:
193 n=999). This effect was also seen in nine other common species (**Table S7**), including *E. coli*
194 (**Fig. 3F**). By contrast, some species like *Bacteroides uniformis* revealed notably lower strain
195 diversity within samples and across time (**Fig. S6D**).

196 The distinction in response to EEN among strains and between closely related species
197 reinforces the importance of strain-level characterization in individuals. Altogether,
198 metagenomic analyses demonstrate that gut microbial communities are dynamic at and below
199 the species level and highly influenced by EEN, motivating us to explore their relationship to
200 the clinical efficacy of EEN.

201 **EEN-like diet triggers protective changes in fecal microbiota**

202 To further evaluate the functional impact of EEN on patient-derived fecal microbiota, we used
203 continuous culture systems in a gut chemostat model and fecal microbiota transfer (FMT) into
204 germ-free (GF) WT and *Il10*$^{-/-}$ mice. *Il10*$^{-/-}$ mice are a microbiota-dependent IBD mouse model
205 responsive to human fecal microbiota, as previously shown for adult CD patients[19] (**Fig. 4A**).
206 The previously used samples from model patients (MP) for the BONCAT experiments were
207 also selected for the transfer experiment (**Fig. 4B, C, I**; **Table S3**, STARMethods).

208 Microbiota transfer of the PreEEN sample of MP1 (MP1-FMT 1, **Fig. 4B,** red arrow) induced
209 colonic tissue inflammation in all gnotobiotic *Il10*$^{-/-}$ mice (histopathology score of 5.3 ± 1.0) but
210 not in WT control mice (**Fig. 4D** $p < 0.001$, histopathology score of 1.3 ± 0.5; **Fig. S7A** H&E),
211 mirroring the active disease state of this patient. Following transfer of MP1 fecal material into
212 the gut chemostat model (MP1-FMT 2, **Fig 4A**), dietary exposure was mimicked using

213 combinations of fiber-free EEN-like (including 10% Modulen IBD® of the 1 kcal/mL
214 preparation) and fiber-repleted (FR) medium, respectively (**Fig. S8A, B**). We then transferred
215 microbiota (MP1-FMT 3) from the chemostat model exposed to EEN-like medium and thereby
216 reversed the inflammatory phenotype of MP1 in *Il10*$^{-/-}$ mice (**Fig. 4D**, histopathology score of
217 *Il10*$^{-/-}$ mice = 2.5 ± 0.8; WT mice = 1.6 ± 0.5; FMT1 vs FMT 3 *Il10*$^{-/-}$ p <0.001; **Fig. 4F** H&E, **Fig.**
218 **S7A**). Conversely, under fiber-repleted medium conditions MP1-FMT 4 induced IBD-like tissue
219 pathology in four out of six *Il10*$^{-/-}$ mice (**Fig. 4D** histopathology score = 3.7 ± 1.0; **Fig. 4F** H&E,
220 **Fig. S7A**), compared to disease-free WT mice (**Fig. 4D** histopathology score = 1.4 ± 0.5, p =
221 0.0087; **Fig. 4F** H&E, **Fig. S7A**). *Tnf* gene expression confirmed active tissue inflammation
222 with significantly elevated expression levels in *Il10*$^{-/-}$ compared to WT mice (**Fig. 4F** p = 0.0022
223 dist. (distal) colon; **Fig. S7D** p = 0.0152 prox. (proximal) colon). Thus, *ex vivo* EEN-like
224 intervention recapitulated therapeutic functional changes to the microbiota.

225 Transfer of the fecal microbiota from MP2 failed to induce inflammation in *Il10*$^{-/-}$ mice (MP2-
226 FMT 1, **Fig 4E** H&E, **Fig. S7B**), resembling the inactive disease state of the patient. Since the
227 stool sample of MP2 was retrieved under EEN therapy, we started the gut chemostat on EEN-
228 like medium (MP2-FMT 2; **Fig. S8C**). In contrast to MP2-FMT 3 (**Fig. 4E** histopathology score
229 in in *Il10*$^{-/-}$ = 2.0 ± 0.6; WT = 1.0 ± 0.6; **Fig. 4G** H&E**, Fig. S7B**), transfer of FR-conditioned
230 microbiota (MP2-FMT 4) triggered IBD-like colitis, including histopathologic changes and
231 elevated *Tnf* tissue expression (**Fig. 4E**, histopathology score in *Il10*$^{-/-}$ = 4.8 ± 1.9 *vs*. WT = 1.5
232 ± 0.5, p (*Il10*$^{-/-}$ FMT1 *vs*. FMT4) = 0.0004, p (*Il10*$^{-/-}$ FMT3 *vs*. FMT4) = 0.0008 ; **Fig. 4G** H&E,
233 *Tnf* gene expression p = 0.0152 dist. colon; **Fig. S7D** p = 0.0022 prox. colon). Thus, both
234 transfer experiments (MP2-FMT 1 and MP2-FMT 3) demonstrate protective effects of EEN.
235 Reintroduction of fiber (MP2-FMT 4) reverted this protective function, indicative for the risk of
236 relapse in MP2 after EEN cessation (**Fig. 4C**).

237 Next, we introduced an EEN-like mouse diet one week prior to FMT (MP3-FMT 4) to evaluate
238 extended dietary effects in gnotobiotic WT and *Il10*$^{-/-}$ mice (**Fig. 4H**). MP3 had elevated fecal
239 calprotectin levels of 2828 mg/L (**Fig. 4I**, blue arrow) and ongoing mucosal inflammation with
240 endoscopic signs of disease activity (**Fig. 4I**, grey arrow), despite achieving clinical remission
241 under EEN therapy. Accordingly, FMT 1 from MP3 induced severe inflammation in all recipient
242 *Il10*$^{-/-}$ mice (**Fig. 4J** histopathology score in *Il10*$^{-/-}$ = 7.3 ± 0.8 *vs*. WT = 1.3 ± 0.5, p = 0.0022;
243 **Fig. S7C** H&E). In contrast to MP1 and MP2 (**Fig. 4D, E**), EEN-like medium in the chemostat
244 model did not change the inflammatory phenotype in IBD-susceptible mice (MP3-FMT 3, **Fig.**
245 **4J** histopathology score in *Il10*$^{-/-}$ = 6.0 ± 1.3 *vs*. WT = 1.6 ± 1.0, p = 0.0006; **Fig. 4K** H&E, **Fig.**
246 **S7C**; *Tnf* p = 0.0022 for dist. colon and prox. colon; **Fig. S7D**). However, introducing EEN-like
247 diet decreased the level of disease severity after MP3-FMT 4 in most *Il10*$^{-/-}$ mice (**Fig. 4J**
248 histopathology score in EEN-like-fed *Il10*$^{-/-}$ = 3.2 ± 3.1 *vs*. WT = 1.3 ± 0.5, p = n.s.; **Fig. 4K**

249 H&E, *Tnf* p = n.s dist. colon; **Fig. S7C, D,** *Tnf* p = 0.0022 for prox. colon) and significantly
250 reduced disease activity compared to the chow-fed group (**Fig. 3J** FMT 3 *vs*. FMT 4**,**
251 histopathology score in EEN-like-fed *Il10*$^{-/-}$ = 3.2 ± 3.1, p = 0.0271, *Il10*$^{-/-}$ FMT 1 *vs*. FMT 4 p =
252 0.0005**, Fig. 4K** H&E, **Fig. S7C**). An additional sample of MP2 after clinical relapse was tested
253 under conditions of the extended EEN-like feeding (**Fig. S8F**, orange arrow), and contrary to
254 MP3, the MP2 relapse sample was resistant to EEN induced protection (**Fig. S8E-L**). These
255 findings suggest that sustained EEN-like feeding increased the chance to prevent recurrence,
256 but efficacy of repeated EEN decreases with a second course.

257 **Individual strain signatures in gnotobiotic *Il10*$^{-/-}$ mice convey protective function of**
258 **patient's microbiota in response to diet**

259 To investigate bacterial strain profiles responsible for the mouse disease phenotypes (**Fig. 4**),
260 we performed metagenomic analyses of all 54 gnotobiotic *Il10*$^{-/-}$ mice colonized with fecal
261 communities of MP1-MP3 (**Fig. 5A-C,** triangles: red - active disease, green - inactive disease;
262 **Fig. S9A**). Out of 100 strains detected in MP1, 64 were specific to mice with active disease,
263 while only three were specific to inactive disease (**Fig. 5A,** lowest Venn diagram (Vd)). Strains
264 in MP2 mice were skewed towards being specific to inactive disease or shared (**Fig. 5B,** lowest
265 Vd), consistent with lower disease activity in MP2 and fewer mice with active disease. Strains
266 in MP3 mice were skewed towards being specific to active disease, probably due to a higher
267 number of MP3 mice having active disease (**Fig. 5C,** lowest Vd).

268 Motivated by these differences, we next sought to identify species, strains, and metabolites
269 that distinguished active *vs*. inactive *Il10*$^{-/-}$ mice. Dozens of species showed significant
270 differential abundance after the transfer experiments of MP1, MP2 and MP3 (40, 16 and 11,
271 respectively **Fig. 5D-F**) including taxa from the network analyses and BONCAT experiments.
272 Considering all microbiota transfer experiments, we detected 181 species, including 24
273 species shared between MP1-MP3 transfer experiments into *Il10*$^{-/-}$ mice (**Fig. 5G, left** Vd). In
274 contrast, none of the identified species shared any common strain within all (**Fig. 5G,** right Vd),
275 demonstrating that active *vs*. inactive disease states in *Il10*$^{-/-}$ mice are mediated by individually
276 variable strain communities. Linear discriminant analysis Effect Size (LEfSe) determined 47
277 species that were differentially abundant between mice with active *vs*. inactive disease, each
278 with individual strain repertoires in samples from the three different MPs (**Fig. S10A**). In the
279 combined analyses *E. clostridioformis* (zOUT5) and *Bacteroides thetaiotaomicron* (zOUT2,
280 zOTU66) were most dominant in mice with active disease and *Akkermansia muciniphila*
281 (zOUT65) and *Escherichia coli* (zOTU4, zOUT8) were most dominant in mice with active
282 disease (**Fig. S10A**). In addition, 56 species were significantly different in abundance
283 comparing mice under chow vs EEN-like diet (**Fig. S10B**) with previously highlighted strains

284 abundant in both groups, as mice colonized with *ex vivo* EEN-conditioned microbiota received
285 either chow or EEN-like diet. Importance of strain level diversity, is obvious as several species
286 were associated to both, active and inactive mice, in the different MP transfers, but the different
287 strains were responding differently in the model systems (**Fig. 5D-G, S10A**).

288 SPLS-DA of untargeted metabolomics from mouse colon content separated active and inactive
289 mice in the respective transfer experiments independent of dietary exposure (**Fig. S9B-D,**
290 **S10C-F**). Several bile acids (BA) were highlighted as differentially abundant, which was
291 confirmed in the targeted measurement primary taurine conjugated and secondary
292 unconjugated BA (**Fig. S9B, C**). Targeted analyses of Isobutyrate showed highest
293 concentration in mouse feces samples colonized with EEN conditioned microbiota on EEN-
294 like diet (**Fig. S9E**). SPLS-DA of the combined untargeted metabolomics dataset confirmed
295 distinct clusters for active and inactive disease independent of MP1-3 donor samples (**Fig.**
296 **S10F**, **Fig. S11**), suggesting that individual strain profiles convey protective or aggressive
297 responses in the IBD susceptible host (**Fig. S12**). These results clearly demonstrate that
298 despite the model patients having personalized strain composition (**Fig. 5G,** right Vd), disease
299 activity in gnotobiotic mice receiving FMTs was consistently associated with a number of
300 metabolic and species-level taxonomic differences. Furthermore, the differentially abundant
301 species in all humanized mice exhibited unique patterns linked to EEN and its cessation in the
302 CD patient cohort (**Fig. S13**), emphasizing both the clinical relevance of our mouse FMT
303 experiment findings and the individual microbial fingerprint of each patient.

304 In summary, we provide evidence that EEN impacts the individual gut microbiome – EEN
305 therapy in the CD-EEN patients, selected fecal samples from three individuals exposed to
306 MCFAs and EEN-like exposure in a non-host and host environment – leading to individual
307 microbiota changes that are functionally relevant and harboring the capacity to induce or not
308 to induce inflammation in mice. Despite the limited selection of donor samples, of the 16 EEN
309 associated zOUTs from the network analyses, 7 zOTUs were found in significantly different
310 abundant taxa in the mouse experiments (**Fig. 5D-F**) and 8 zOTUs were identified in the
311 BONAT experiments (**Fig 2E, S5D**), suggesting a direct link of MCFAs in EEN to changes in
312 the fecal microbiota of CD patients. The microbiota transfer studies in the gut chemostat model
313 provides proof-of-concept that microbiota changes are functionally relevant and diet shapes
314 individual microbiota signatures harboring the capacity to induce or not to induce inflammation
315 in mice. In conclusion, we provide evidence that EEN therapy creates explicit functional
316 changes of temporally and individually variable microbiome profiles in CD patients. These data
317 challenge the concept that protective microbiome signatures are universal to patients and
318 therapeutic interventions, instead we postulate individually diverse microbiome signatures with
319 shared functional properties under these therapeutic conditions.

320 **Discussion**

321 We followed 78 pediatric IBD patients longitudinally, focusing on 20 newly diagnosed CD
322 patients receiving EEN as first-line treatment. Our results corroborate previous observations
323 that EEN is highly effective at inducing remission. We demonstrate that protective functions of
324 EEN therapy are mediated through diet-induced changes in patient microbiomes despite
325 considerable variations in individual microbiota over time. Dietary exposure of EEN
326 components like MCFAs and EEN-like diets on individual patient-derived fecal microbiota
327 modified the activity and function of selective taxa. EEN mediated changes of fecal bacteria in
328 the chemostat models convey anti-inflammatory phenotypes after FMT into IBD-relevant GF
329 mice, strongly supporting a causal role of EEN-mediated protective changes in the
330 microbiome. In contrast, fiber-repleted diets antagonized these protective functions. Notably
331 and based on the model conditions, we identify patient-specific species and strain signatures
332 in response to EEN therapy, confirming the highly personalized strain-level dynamics in
333 patients and the absence of universal protective signatures.

334 Longitudinal sampling revealed an integrated network of taxonomic and metabolomic
335 signatures across pediatric CD patients. In line with previous findings[20], EEN therapy was
336 associated with the genus *Enterocloster* (Lachnospiraceae; former genus *Lachnoclostridium)*.
337 In addition, several *Enterocloster* species responded to MCFA exposure, *E. clostridioformis*
338 (zOUT5) was the most abundant species in inactive *Il10*$^{-/-}$ mice and showed high dynamics in
339 the CD-EEN cohort together with *E. bolteae* (zOTU5). Low levels of *Lachnoclostridium* have
340 been associated with CD[21], supporting a protective function of *Enterocloster* in response to
341 EEN therapy. Nevertheless, taxonomic shifts at the cessation of EEN were highly patient-
342 specific. For example, while in the majority of patients, *E. bolteae* (zOTU5) was at much higher
343 relative abundance during EEN compared to PostEEN, the dominant strains in many patients
344 changed over this transition, and most strains were detected in just one subject. This individual
345 diversity and turnover contribute to challenges in predicting taxonomic responses to dietary
346 changes globally. Antibiotics and pre-existing dysbiosis are both associated with increased
347 strain engraftment in patients receiving fecal microbiota transplants[22]. Likewise, the
348 microbiome perturbation caused by EEN - and its cessation - may encourage strain turnover
349 in some species, with potentially complex consequences for microbial function after therapy.
350 Beyond taxonomic alterations, we highlighted six metabolites associated with EEN treatment
351 and 16 metabolites associated with PostEEN samples. Independently, metagenomic analysis
352 highlighted 583 bacterial gene functions with substantial changes in response to EEN,
353 suggesting specific metabolic adaptations of the microbiota to host diets. Modulen IBD® is
354 characterized by easily digestible carbohydrates and high fat content, including medium-chain
355 triglycerides[9]. Our integrated network analysis highlighted caprylic (C8:0), decanoic (C10:0),
356 and lauric (C12:0) acids as associated with EEN. MCFAs are part of the EEN formula and

357 mediate anti-bacterial and anti-inflammatory functions[23–25]. The exposure of LA, DA and OA to
358 selected patient samples directly link nutritional components of EEN to selectively activated
359 taxa in the microbiota of CD patients. Surprisingly, from the limited selection of donor samples,
360 50% (8 out of 16 zOTUs) of the EEN associated bacteria significantly responded in the
361 BONCAT experiments. Diets high in fat trigger release of bile acids[26], providing a rationale for
362 *C. innocuum* and *Hungatella hathewayi* to be associated with EEN [27,28]. Concordantly, our
363 untargeted metabolomics analysis identified several bile acids as differentially abundant,
364 highlighting a potential microbial conversion of primary to secondary bile acids in non-inflamed
365 *Il10*$^{-/-}$ mice, potentially promoting wound healing and epithelial regeneration[26]. In a recent study
366 (FARMM), EEN specifically affected amino acid pathways in the microbiome creating a
367 metabolite milieu low in bacteria-derived indoles[17], which was also low abundant in the EEN-
368 like mouse diet. In addition, EEN-related protective effects in *Il10*$^{-/-}$ mice are partially mediated
369 by Isobutyrate production[16], which was highest in mice receiving EEN-conditioned microbiota
370 on EEN-like diet, supporting the hypothesis that microbiota and metabolite changes contribute
371 to the EEN therapeutic efficacy.

372 In healthy humans, dietary fiber intake supports beneficial functions of the gastrointestinal
373 tract[29]. In animal models, low fiber diets induce adverse microbiota changes associated with
374 impaired intestinal barrier integrity and bacteria-related mucus degradation[30,31], highlighting
375 the fiber paradox in understanding EEN-mediated anti-inflammatory mechanisms in IBD.
376 Dietary fiber consists of complex carbohydrates, which are resistant to digestion and
377 absorption by the host. However, dietary fiber degradation and availability for the host depends
378 on the fermenting potential of host-specific microbial communities, which are modified by
379 intestinal inflammation[29,32–34]. Using the combined gut chemostat-to-mouse transfer approach,
380 we showed that a fiber-free EEN-like medium maintains the anti-inflammatory and remitting
381 phenotype associated with EEN therapy. Concordantly, the protective effect of EEN-
382 conditioned microbiota is reversible upon exposure to fiber-repleted diet, as a proxy for regular
383 diet PreEEN and PostEEN, and potentially resistant to repetitive EEN as shown before[12]. A
384 potentially adverse effect of fiber in IBD was elucidated by Armstrong and colleagues,
385 demonstrating the incapability and loss of function of bacteria to degrade fibers promoting
386 intestinal inflammation[34]. Furthermore, several additional studies link the presence of dietary
387 fiber with increased inflammation[35,36]. In addition, fiber-free diets prevent and diminish the
388 colonization of identified pathobionts in different CD-like mouse models[37,38], supporting our
389 hypothesis that EEN therapy directly creates protective niches in the gut microbiome.
390 Preserving a beneficial microbiome after cessation of EEN may be a new approach to guide
391 mucosal healing and remission in pediatric CD[39]. In our IBD cohort, 40% (8/20) of pediatric CD
392 patients relapsed within the first year after EEN treatment, highlighting the necessity to
393 maintain remitting conditions. Our data clearly demonstrate that EEN therapy mediates

394 protective changes in individually variant microbiome profiles, leading towards personalized
395 patient-to-patient species and strain signatures. These findings support the idea to develop
396 patient-tailored maintenance strategies in pediatric CD involving combinations of personalized
397 nutritional and bacterial interventions.

398 **Acknowledgement**

399 We thank the patients and their families for participating in our research.

400 **Author contribution**

401 DHaller and TS are responsible for the conceptual design of the study; DHäcker and DHaller
402 designed the *ex vivo* experiments; KSiebert, HHölz, JHeetmeyer, FDeZen, GLeThi, TS:
403 collected and prepared clinical data and samples, accompanied, followed and characterized
404 patients, analysis of clinical data; HHölz, TS recruited patients; DHäcker, HHeimes, AMetwaly
405 and DHaller performed and interpreted mouse and fermenter experiments; AR and JN
406 performed BONCAT experiments and analyses; DHäcker performed 16S rRNA gene amplicon
407 and corresponding statistical analysis with support of QM and ML; CM, QM, KSocas, ML, KK
408 performed metabolomics with statistical analysis; KSiebert, DHäcker, NK, AMetwaly, ML
409 responsible for integration of clinical metadata with 16S and metabolomics as well as sample
410 selection and performance of data integration and network analysis; NK, ML, PJK performed
411 16S & untargeted metabolomics data integration, untargeted metabolomics data analyses; BS,
412 AMahapatra, KSP performed metagenomic sequencing and analyses; KN provided 16S rRNA
413 gene amplicon and metagenome sequencing and support for analysis; DHäcker, KSiebert, BS,
414 NK, KSP, TS and DHaller evaluated and interpreted data and wrote the manuscript; All authors
415 provided input on the manuscript, critically revised and approved the final version of the
416 manuscript.

417 **Funding**

418 Funded by the Deutsche Forschungsgemeinschaft (DFG, German Research Foundation) –
419 project number 395357507 (SFB 1371, Microbiome Signatures) and The Leona M. and Harry
420 B. Helmsley Charitable Trust (project numbers 2847 and 2304-05970). TS is supported by the
421 Medical & Clinician Scientist Program (MCSP) of the Faculty of Medicine at LMU Munich.
422 Salary for DHäcker was supported by the National Research Foundation, Prime Minister's
423 Office, Singapore under its Campus for Research Excellence and Technological Enterprise
424 (CREATE) programe.

425 **Conflict of interest**

426 DHaller served on the Microbiome Expert Panel from Reckitt Benckiser Health Limited. TS
427 received lecture honoraria from Nutricia and MSD and travel support from Abbvie and Ferring
428 outside the submitted work.

429

ORCID IDs

Deborah Häcker https://orcid.org/0000-0001-7914-9470
Kolja Siebert https://orcid.org/0009-0005-8083-7074
Byron J Smith https://orcid.org/0000-0002-0182-404X
Nikolai Köhler https://orcid.org/0000-0002-5103-883X
Alessandra Riva https://orcid.org/0000-0002-5724-7616
Aritra Mahapatra https://orcid.org/0000-0003-0078-8590
Jiatong Nie https://orcid.org/0009-0007-3192-0095
Amira Metwaly https://orcid.org/0000-0001-5740-0230
Hannes Hoelz https://orcid.org/0000-0002-7208-6195
Quirin Manz https://orcid.org/0000-0002-5706-2718
Jeannine Heetmeyer https://orcid.org/0000-0002-0599-9613
Katharina Socas https://orcid.org/0009-0003-8625-4879
Giang Le Thi https://orcid.org/0000-0002-2504-9551
Chen Meng https://orcid.org/0000-0002-5968-6719
Karin Kleigrewe https://orcid.org/0000-0002-7718-0252
Klaus Neuhaus https://orcid.org/0000-0002-6020-2814
Markus List https://orcid.org/0000-0002-0941-4168
Katherine S Pollard https://orcid.org/0000-0002-9870-6196
Tobias Schwerd https://orcid.org/0000-0002-2281-4852
Dirk Haller http://orcid.org/0000-0002-6977-4085

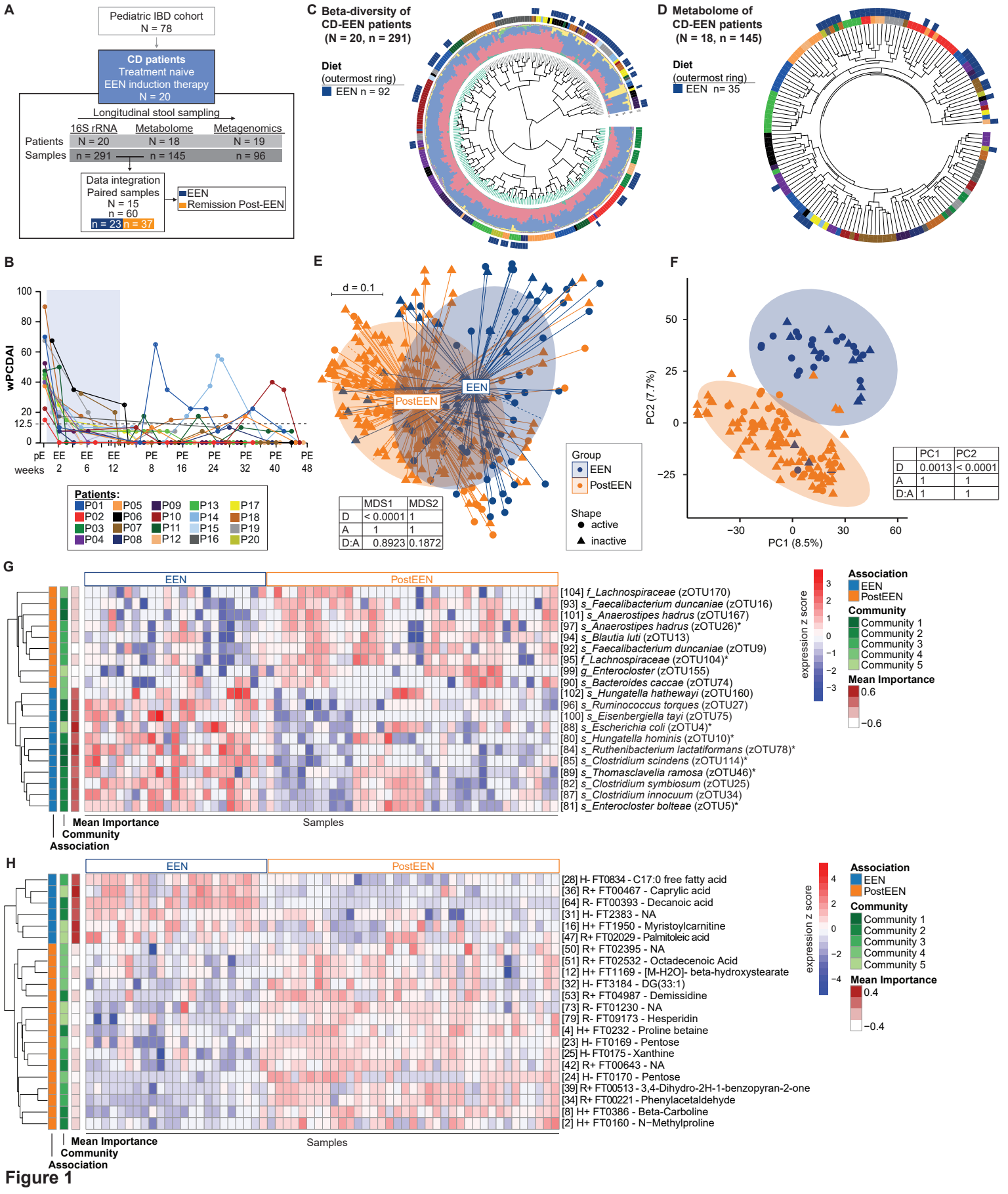
A
Pediatric IBD cohort
N = 78
CD patients
Treatment naive
EEN induction therapy
N = 20
Longitudinal stool sampling
16S rRNA
Metabolome
Metagenomics
Patients
N = 20
N = 18
N = 19
Samples
n = 291
n = 145
n = 96
Data integration
Paired samples
N = 15
n = 60
n = 23
n = 37
EEN
Remission Post-EEN
B
wPCDAI
weeks
pE
EE 2
EE 6
EE 12
PE 8
PE 16
PE 24
PE 32
PE 40
PE 48
Patients:
P01 P05 P09 P13 P17
P02 P06 P10 P14 P18
P03 P07 P11 P15 P19
P04 P08 P12 P16 P20
C
Beta-diversity of CD-EEN patients (N = 20, n = 291)
Diet (outermost ring)
EEN n = 92
D
Metabolome of CD-EEN patients (N = 18, n = 145)
Diet (outermost ring)
EEN n= 35
E
d = 0.1
EEN
PostEEN
MDS1 MDS2
D < 0.0001 1
A 1 1
D:A 0.8923 0.1872
Group
EEN
PostEEN
Shape
active
inactive
F
PC2 (7.7%)
PC1 (8.5%)
PC1 PC2
D 0.0013 < 0.0001
A 1 1
D:A 1 1
G
EEN
PostEEN
[104] f_Lachnospiraceae (zOTU170)
[93] s_Faecalibacterium duncaniae (zOTU16)
[101] s_Anaerostipes hadrus (zOTU167)
[97] s_Anaerostipes hadrus (zOTU26)*
[94] s_Blautia luti (zOTU13)
[92] s_Faecalibacterium duncaniae (zOTU9)
[95] f_Lachnospiraceae (zOTU104)*
[99] g_Enterocloster (zOTU155)
[90] s_Bacteroides caccae (zOTU74)
[102] s_Hungatella hathewayi (zOTU160)
[96] s_Ruminococcus torques (zOTU27)
[100] s_Eisenbergiella tayi (zOTU75)
[88] s_Escherichia coli (zOTU4)*
[80] s_Hungatella hominis (zOTU10)*
[84] s_Ruthenibacterium lactatiformans (zOTU78)*
[85] s_Clostridium scindens (zOTU114)*
[89] s_Thomasclavelia ramosa (zOTU46)*
[82] s_Clostridium symbiosum (zOTU25)
[87] s_Clostridium innocuum (zOTU34)
[81] s_Enterocloster bolteae (zOTU5)*
Mean Importance
Community
Association
Samples
expression z score
Association
EEN
PostEEN
Community
Community 1
Community 2
Community 3
Community 4
Community 5
Mean Importance
0.6
−0.6
H
EEN
PostEEN
[28] H- FT0834 - C17:0 free fatty acid
[36] R+ FT00467 - Caprylic acid
[64] R- FT00393 - Decanoic acid
[31] H- FT2383 - NA
[16] H+ FT1950 - Myristoylcarnitine
[47] R+ FT02029 - Palmitoleic acid
[50] R+ FT02395 - NA
[51] R+ FT02532 - Octadecenoic Acid
[12] H+ FT1169 - [M-H2O]- beta-hydroxystearate
[32] H- FT3184 - DG(33:1)
[53] R+ FT04987 - Demissidine
[73] R- FT01230 - NA
[79] R- FT09173 - Hesperidin
[4] H+ FT0232 - Proline betaine
[23] H- FT0169 - Pentose
[25] H- FT0175 - Xanthine
[42] R+ FT00643 - NA
[24] H- FT0170 - Pentose
[39] R+ FT00513 - 3,4-Dihydro-2H-1-benzopyran-2-one
[34] R+ FT00221 - Phenylacetaldehyde
[8] H+ FT0386 - Beta-Carboline
[2] H+ FT0160 - N−Methylproline
Mean Importance
Community
Association
Samples
expression z score
Association
EEN
PostEEN
Community
Community 1
Community 2
Community 3
Community 4
Community 5
Mean Importance
0.4
−0.4

Figure 1

451 ## Figures

452 ***Figure 1: Fecal microbial and metabolic changes in response to EEN.***
453 *Patients of the Pediatric IBD cohort with focus on 20 newly diagnosed and treatment naïve CD patients, receiving*
454 *EEN induction therapy. Longitudinal collected samples (n = samples, N = patients) that were used for 16S rRNA*
455 *amplicon and metagenomic sequencing as well as metabolome analysis are shown. Paired samples (n = 60) were*
456 *used for data integration of 16S rRNA and metabolome data (samples highlighted in blue = taken under EEN,*
457 *orange = taken PostEEN).* ***B*** *Weighted pediatric Crohn's Disease activity index (wPCDAI) over time (EEN shaded*
458 *blue), remission achieved below 12.5 points (dashed line). pE = PreEEN, EE = EEN, PE = PostEEN.* ***C*** *Beta-*
459 *diversity analysis of the fecal microbiota samples. The circular dendrogram shows differences in beta-diversities*
460 *from the longitudinal microbial profiling based on generalized UniFrac distances between the 291 stool samples of*
461 *the 20 patients. Indicated in color code are the patients and samples collected during EEN. Color code of taxonomic*
462 *composition at phylum level as in B. Branch color indicates results of unsupervised clustering. Patient colour code*
463 *found in B.* ***D*** *Visualization of untargeted metabolome samples from 18 newly diagnosed pediatric CD patients*
464 *receiving EEN therapy: Complete clustering with Euclidean distance of longitudinal samples from 18 CD-EEN*
465 *patients (n = 145), Patient colour code found in B.* ***E*** *Beta-diversity MDS plot samples during EEN (n = 89, active:*
466 *55, inactive: 34) vs. PostEEN (n = 188, active: 41, inactive: 147).* ***F*** *Analyses of untargeted metabolomics with*
467 *representative PCA plot comparing samples during EEN (n = 35, active: 21, inactive: 14) and PostEEN (n = 106*
468 *active: 21, inactive: 85). Axes indicate principal components (PC), with PC1 representing the most variation (%)*
469 *and PC2 representing the second most variation (%). (**E, F**) Coefficients were tested with a t-test, reported p-values*
470 *are Bonferroni-corrected, D = diet, A = activity, D:A = interaction term between diet and activity.* ***G, H*** *Heatmaps*
471 *depicting the abundances of the top selected feature from the correlation network Supplementary Fig. S2. Selected*
472 *sPLS-DA features were subsetted by their mean importance (see Star Methods: Data integration of 16s rRNA*
473 *amplicon data with metabolomics and metagenomics for details). All values shown are feature-wise z-scores.*
474 *Information on association with EEN (blue), PostEEN (orange), sample collection under which diet (EEN blue),*
475 *PostEEN (orange), community association (1 – 5) are indicated;* ***G*** *zOTUs,*BONCAT responders Fig.2,* ***H***
476 *Metabolites.*

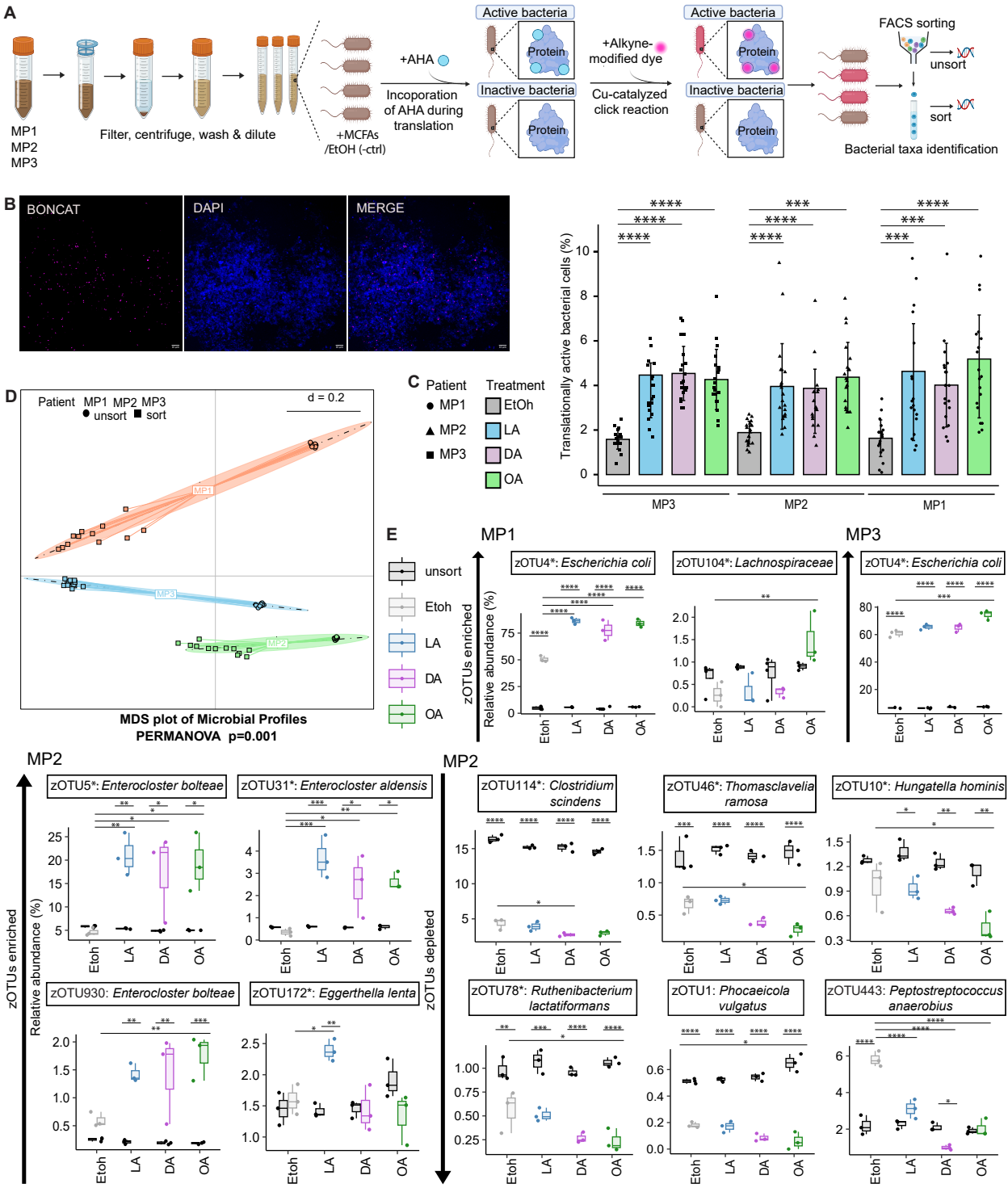
A
MP1
MP2
MP3
Filter, centrifuge, wash & dilute
+MCFAs /EtOH (-ctrl)
+AHA
Incoporation of AHA during translation
Active bacteria
Protein
Inactive bacteria
Protein
+Alkyne-modified dye
Cu-catalyzed click reaction
Active bacteria
Protein
Inactive bacteria
Protein
FACS sorting
unsort
sort
Bacterial taxa identification
B
BONCAT
DAPI
MERGE
Translationally active bacterial cells (%)
MP3
MP2
MP1
C
Patient
MP1
MP2
MP3
Treatment
EtOh
LA
DA
OA
D
Patient MP1 MP2 MP3
unsort sort
d = 0.2
MP1
MP3
MP2
MDS plot of Microbial Profiles
PERMANOVA p=0.001
E
unsort
Etoh
LA
DA
OA
MP1
MP3
zOTUs enriched
Relative abundance (%)
zOTU4*: Escherichia coli
zOTU104*: Lachnospiraceae
zOTU4*: Escherichia coli
MP2
zOTUs enriched
zOTUs depleted
zOTU5*: Enterocloster bolteae
zOTU31*: Enterocloster aldensis
zOTU930: Enterocloster bolteae
zOTU172*: Eggerthella lenta
zOTU114*: Clostridium scindens
zOTU46*: Thomasclavelia ramosa
zOTU10*: Hungatella hominis
zOTU78*: Ruthenibacterium lactatiformans
zOTU1: Phocaeicola vulgatus
zOTU443: Peptostreptococcus anaerobius

Figure 2

477 ***Figure 2: MCFAs-Induced Activation of Translationally Active Gut Bacteria.***
478 ***A*** *Experimental design. MP1, MP2 and MP3 stool samples previously stored in glycerol, were incubated under*
479 *anaerobic conditions and in the presence of medium chain fatty acids (MCFA)[(lauric acid (LA), decanoic acid (DA)*
480 *and octanoic acid (OA)] and of the cellular activity marker (L-Azidohomoalanine (AHA). Translationally active*
481 *bacterial cells labelled with alkyne-modified dye were sorted with BONCAT-FACS. The taxonomic profiles of sorted*
482 *and unsorted cells were identified by 16S rRNA genes amplicon sequencing.* ***B*** *Representative confocal*
483 *microscopic images of one stool samples (MP2) stimulated with OA. Pink: active cells (BONCAT-Cy5); Blue: all*
484 *cells (DAPI). Scale bar is 10µm.* ***C*** *Translationally active bacterial cells quantified in MP1, MP2 and MP3 patients.*
485 *P values were calculated by Kruskal-Wallis test and Dunn test for multiple comparisons. *p < 0.05, **p < 0.01, ***p*
486 *< 0.001, ****p < 0.0001.* ***D*** *Beta-diversity MDS plots shows clustering of samples based on model patients and*
487 *sorted-unsorted groups (perMANOVA p=0.001 for both comparisons). MP1 = orange, MP2 = green, MP3 =*
488 *turquoise, sorted cells = square, unsorted cells = circle.* ***E*** *Relative abundances of significant enriched and depleted*
489 *zOTUs in MP1, MP2 and MP3. *zOUTs identified in Network analyses Fig 1G, S2. P values were calculated by*
490 *ANOVA and Tukey's test for multiple comparisons. *p < 0.05, **p < 0.01, ***p < 0.001, ****p < 0.0001.*

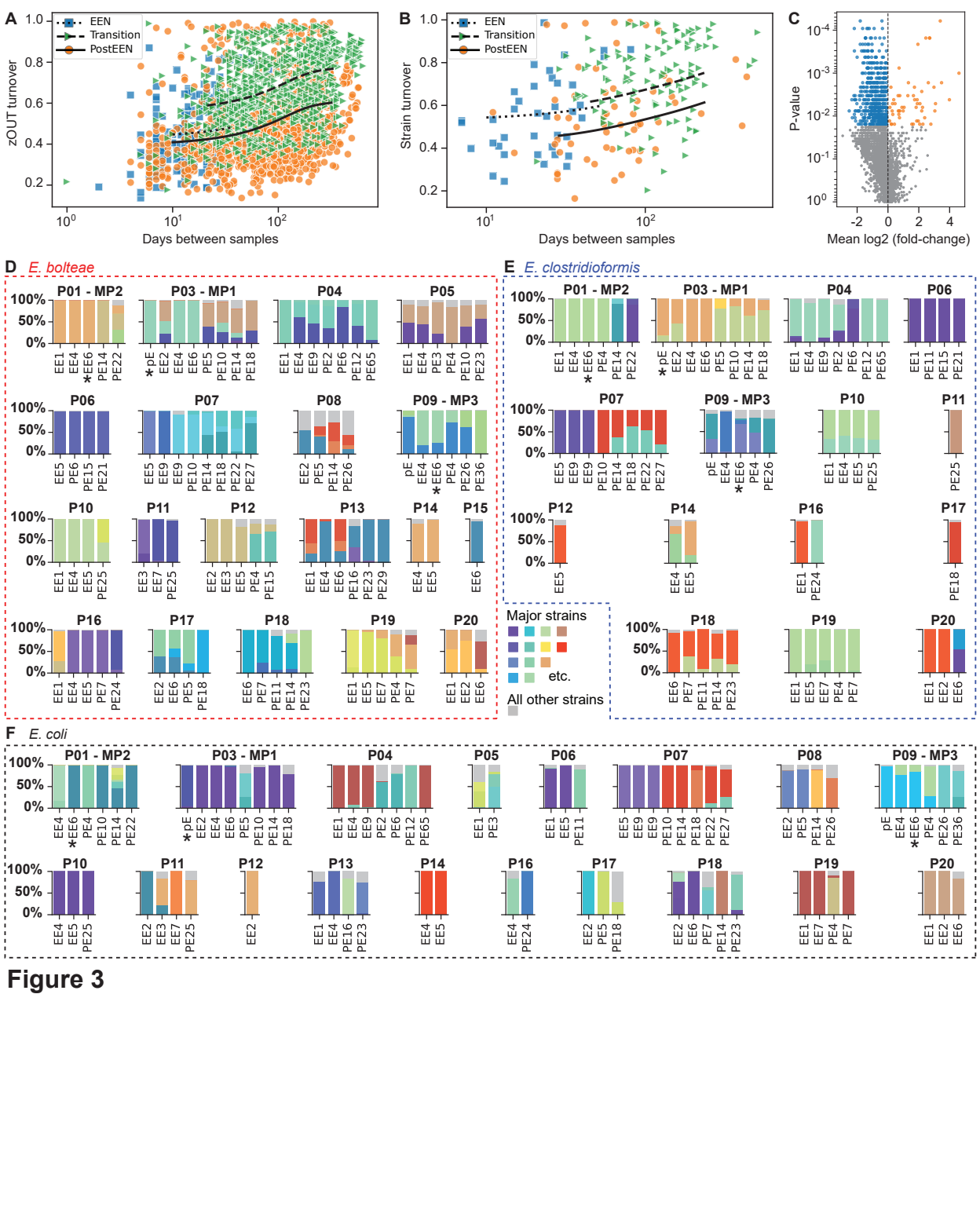
A
EEN
Transition
PostEEN
zOUT turnover
Days between samples
B
Strain turnover
C
P-value
Mean log2 (fold-change)
D E. bolteae
E E. clostridioformis
Major strains
etc.
All other strains
F E. coli

Figure 3

491 ***Figure 3: Species and strain turnover during the transition off of EEN:***
492 ***A, B*** *Turnover of taxonomic composition during the transition from EEN to a PostEEN diet of both* ***(A)*** *zOTU and*
493 ***(B)*** *strain compositions. The three lines reflect cubic spline regression of Bray-Curtis dissimilarities against time,*
494 *averaged across subjects and offset by an independent intercept for each pair type.* ***C*** *Volcano plots showing COGs*
495 *with significant changes in normalized abundance at the transition off of EEN (Wilcoxon test at false discovery rate*
496 *(FDR) < 0.1). Here, 54 COGs were at significantly greater relative depth during PostEEN (orange points) and 529*
497 *during EEN (blue).* ***D-F****. Composition over time of strains within* ***(D)*** *E. bolteae (red box),* ***(E)*** *E. clostridioformis (blue*
498 *box),* ***(F)*** *E. coli (black box) all three abundant in the CD-EEN patients: All three species have notable strain*
499 *dynamics during and after EEN. Strain genotypes and fractions were estimated from shotgun metagenomic data.*
500 *Fractions of abundant strains (colored bars) are shown across samples from individual subjects (P01, P02…),*
501 *before EEN ("pE" labels on x-axis), during ("EE") and after ("PE"). *Samples used as donor samples in other*
502 *experiments. Strain fractions for the species sum to 1; minor strains are summed together and shown in grey. An*
503 *analogous plot for B. uniformis is in Supplementary Figure S4D.*

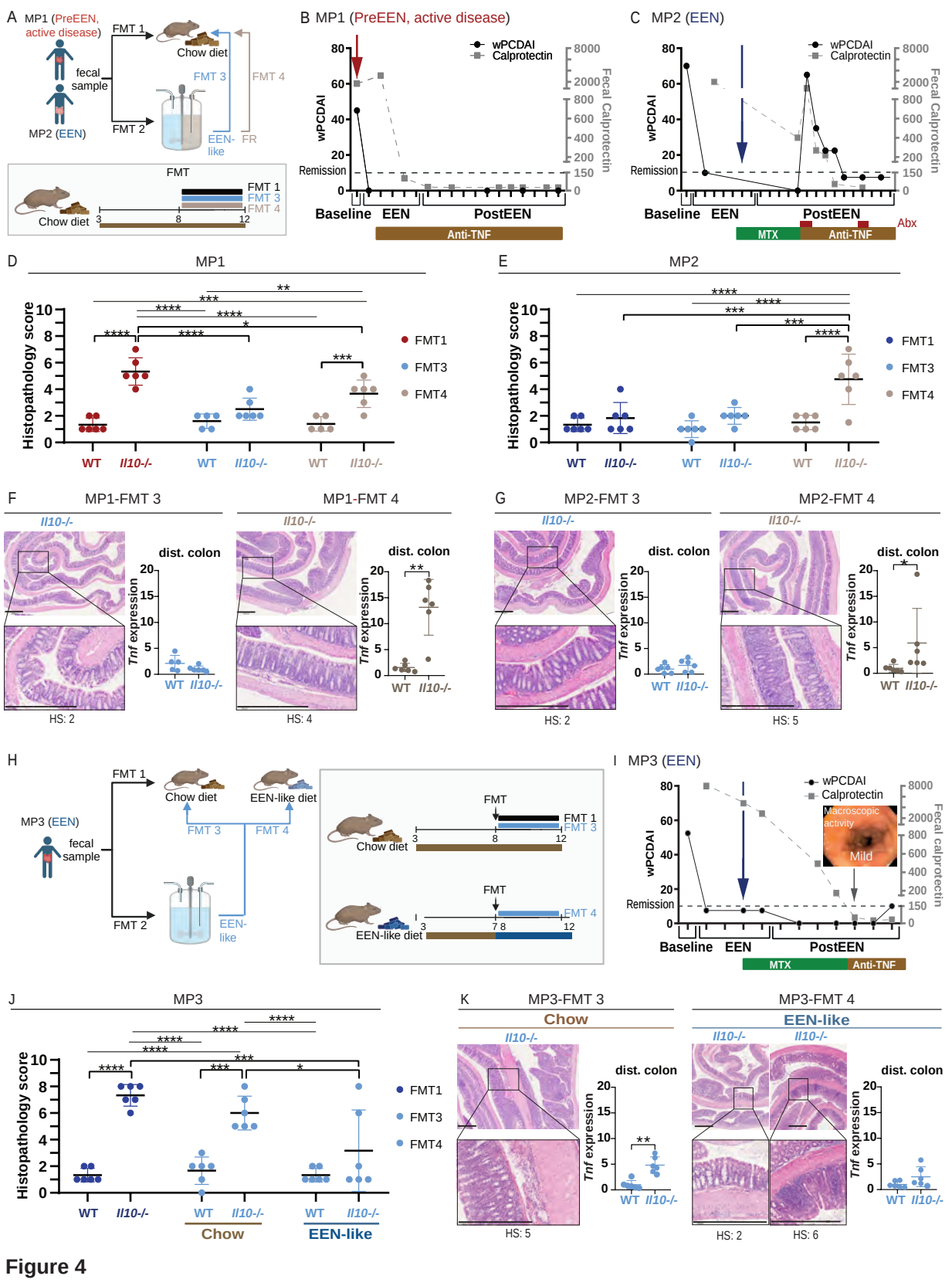
A
MP1 (PreEEN, active disease)
fecal sample
MP2 (EEN)
FMT 1
FMT 2
Chow diet
FMT 3
FMT 4
EEN-like
FR
FMT
Chow diet
B MP1 (PreEEN, active disease)
wPCDAI
Calprotectin
Fecal Calprotectin
Remission
Baseline
EEN
PostEEN
Anti-TNF
C MP2 (EEN)
MTX
Abx
D MP1
Histopathology score
FMT1
FMT3
FMT4
WT
Il10-/-
E MP2
F MP1-FMT 3
MP1-FMT 4
dist. colon
Tnf expression
HS: 2
HS: 4
G MP2-FMT 3
MP2-FMT 4
HS: 5
H
MP3 (EEN)
EEN-like diet
I MP3 (EEN)
Macroscopic activity
Mild
J MP3
Chow
EEN-like
K MP3-FMT 3
MP3-FMT 4
HS: 6

Figure 4

Figure 4: Functional validation of gut microbiota-dependent EEN-efficacy using* ex vivo *fermentation and gnotobiotic humanized mice.

A *Experimental scheme: FMT 1, Patient sample is transferred into GF mice at the age of 8 weeks for 4 weeks. Same patient sample is also transferred (FMT 2) in an* ex vivo *gut chemostat model and treated with medium simulating EEN (EEN-like, devoid of fibers) or a regular diet (fiber-rich, FR). Fermented sample is transferred (post* ex vivo*) into GF mice (age of 8 weeks) for 4 weeks (FMT 3 - EEN-like medium conditioned, FMT 4 - FR medium conditioned).* ***B, C*** *Transfer of patient sample: patients disease state with wPCDAI and fecal calprotectin levels, therapy response over time with maintenance therapy (MTX, Anti-TNF) and sampling time point.* ***B*** *Model Patient (MP) 1, sample (red arrow) collected PreEEN in active disease.* ***C*** *MP2, sample (blue arrow) collected in EEN induced remission.* ***D*** *Mouse histopathology scoring of colon Swiss roles of FMT 1, 3 and 4 from MP1.* ***E*** *Mouse histopathology scoring of colon Swiss roles of FMT 1, 3 and 4 from MP2.* ***F, G*** *Mouse transfer experiments from FMT 3 and 4: Representative (mean of group) H&E stained sections of colonic Swiss roles and corresponding higher magnifications for Il10$^{-/-}$ mice (scale bars = 500 µM, HS = histopathology score) respective controls in Extended Data Fig 3) with* Tnf *gene expression levels (fold of control) in distal colon.* ***F*** *MP1.* ***G*** *MP2.* ***H*** *Experimental scheme: Patient sample from MP3 is transferred into GF mice (FMT 1) at the age of 8 weeks, for 4 weeks. Same patient sample is also transferred in an* ex vivo *gut chemostat model and treated with EEN-like medium. Fermented sample is transplanted (post* ex vivo*) into GF mice at the age of 8 weeks, for 4 weeks getting either chow diet (FMT 3) or EEN-like purified diet (EEN-like) one week prior to FMT (FMT 4).* ***I*** *MP3 sample for transfer (EEN): patients' disease state with wPCDAI and fecal calprotectin, therapy response over time, maintenance therapy (MTX, Anti-TNF) and sampling time point of transferred fecal sample (blue arrow); grey arrow indicates endoscopy performed in the patient PostEEN and the picture taken during endoscopy shows active ileitis.* ***J*** *Mouse histopathology scoring of colon Swiss roles of FMT 1, 3 and 4 from MP3.* ***K*** *Mouse transfer experiments from FMT 3 and 4 from MP3: Representative (mean of group) H&E stained sections of colonic Swiss roles and corresponding higher magnifications for Il10$^{-/-}$ mice (scale bars = 500 µM, HS = histopathology score) respective controls in Extended Data Fig 3) with* Tnf *gene expression levels (fold of control) in distal colon.* ***A, H*** *Created with BioRender.com. Data are represented by (**D, E, F, G, J, K**) mean ± SD of six biological replicates. P values were calculated by Mann-Whitney test (**F, G, K**) or two-way ANOVA with Tukey multiple pairwise-comparisons test (**D, E, J**). *p < 0.05, **p < 0.01, ***p < 0.001, ****p < 0.0001*

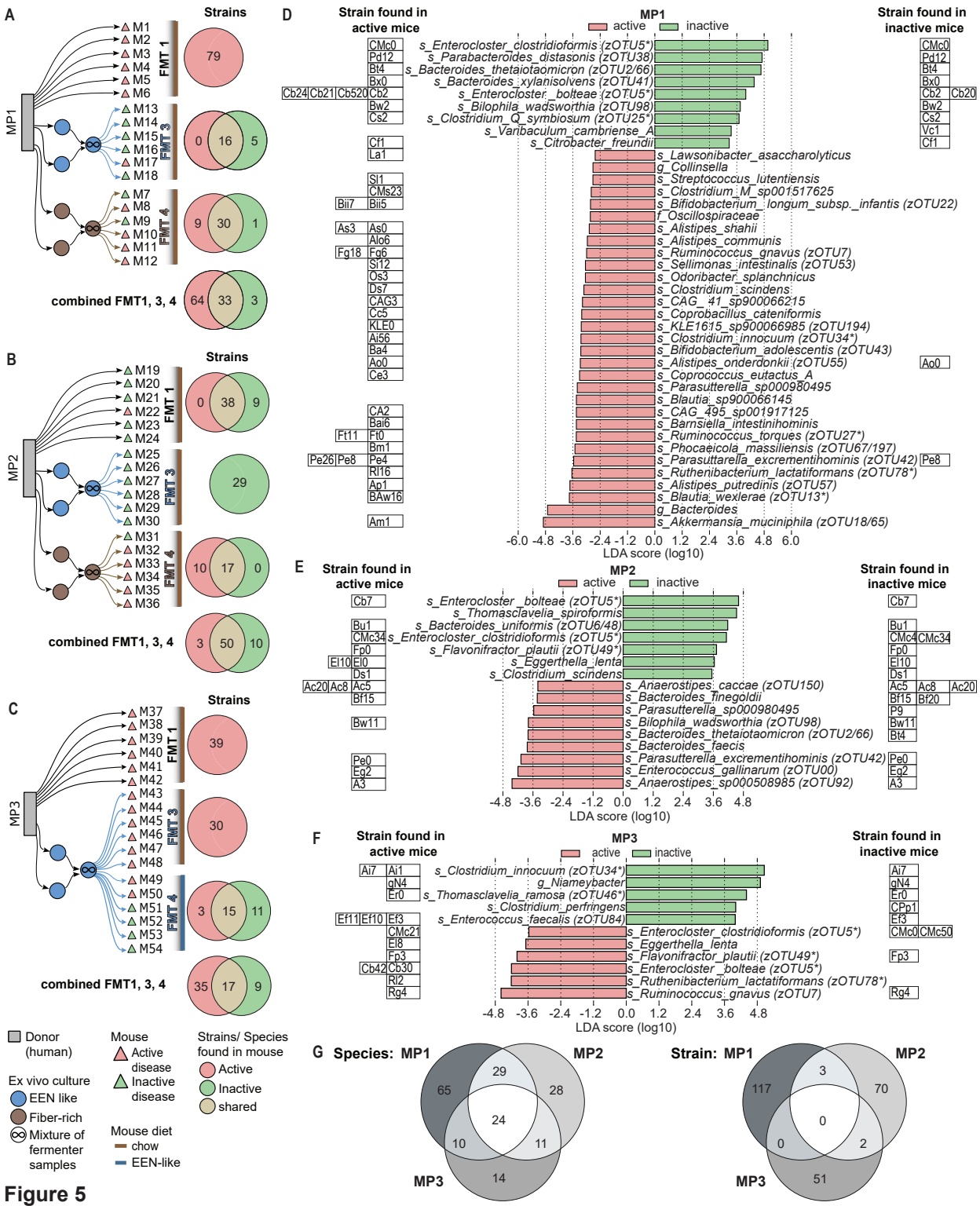
A
Strains
MP1
M1
M2
M3
M4
M5
M6
FMT 1
79
M13
M14
M15
M16
M17
M18
FMT 3
0
16
5
M7
M8
M9
M10
M11
M12
FMT 4
9
30
1
combined FMT1, 3, 4
64
33
3
B
Strains
MP2
M19
M20
M21
M22
M23
M24
FMT 1
0
38
9
M25
M26
M27
M28
M29
M30
FMT 3
29
M31
M32
M33
M34
M35
M36
FMT 4
10
17
0
combined FMT1, 3, 4
3
50
10
C
Strains
MP3
M37
M38
M39
M40
M41
M42
FMT 1
39
M43
M44
M45
M46
M47
M48
FMT 3
30
M49
M50
M51
M52
M53
M54
FMT 4
3
15
11
combined FMT1, 3, 4
35
17
9
D
Strain found in active mice
MP1
active
inactive
Strain found in inactive mice
CMc0
Pd12
Bt4
Bx0
Cb24 Cb21 Cb520 Cb2
Bw2
Cs2
Cf1
La1
Sl1
CMs23
Bii7 Bii5
As3 As0
Alo6
Fg18 Fg6
Sl12
Os3
Ds7
CAG3
Cc5
KLE0
Ai56
Ba4
Ao0
Ce3
CA2
Bai6
Ft11 Ft0
Bm1
Pe26 Pe8 Pe4
Rl16
Ap1
BAw16
Am1
s_Enterocloster_clostridioformis (zOTU5*)
s_Parabacteroides_distasonis (zOTU38)
s_Bacteroides_thetaiotaomicron (zOTU2/66)
s_Bacteroides_xylanisolvens (zOTU41)
s_Enterocloster_bolteae (zOTU5*)
s_Bilophila_wadsworthia (zOTU98)
s_Clostridium_Q_symbiosum (zOTU25*)
s_Varibaculum_cambriense_A
s_Citrobacter_freundii
s_Lawsonibacter_asaccharolyticus
g_Collinsella
s_Streptococcus_lutentiensis
s_Clostridium_M_sp001517625
s_Bifidobacterium_longum_subsp._infantis (zOTU22)
f_Oscillospiraceae
s_Alistipes_shahii
s_Alistipes_communis
s_Ruminococcus_gnavus (zOTU7)
s_Sellimonas_intestinalis (zOTU53)
s_Odoribacter_splanchnicus
s_Clostridium_scindens
s_CAG_41_sp900066215
s_Coprobacillus_cateniformis
s_KLE1615_sp900066985 (zOTU194)
s_Clostridium_innocuum (zOTU34*)
s_Bifidobacterium_adolescentis (zOTU43)
s_Alistipes_onderdonkii (zOTU55)
s_Coprococcus_eutactus_A
s_Parasutterella_sp000980495
s_Blautia_sp900066145
s_CAG_495_sp001917125
s_Barnsiella_intestinihominis
s_Ruminococcus_torques (zOTU27*)
s_Phocaeicola_massiliensis (zOTU67/197)
s_Parasuttarella_excrementihominis (zOTU42)
s_Ruthenibacterium_lactatiformans (zOTU78*)
s_Alistipes_putredinis (zOTU57)
s_Blautia_wexlerae (zOTU13*)
g_Bacteroides
s_Akkermansia_muciniphila (zOTU18/65)
Ao0
Pe8
-6.0 -4.8 -3.6 -2.4 -1.2 0.0 1.2 2.4 3.6 4.8 6.0
LDA score (log10)
E
Strain found in active mice
MP2
active
inactive
Strain found in inactive mice
Cb7
Bu1
CMc34
Fp0
El10 El0
Ds1
Ac20 Ac8 Ac5
Bf15
Bw11
Pe0
Eg2
A3
s_Enterocloster_bolteae (zOTU5*)
s_Thomasclavelia_spiroformis
s_Bacteroides_uniformis (zOTU6/48)
s_Enterocloster_clostridioformis (zOTU5*)
s_Flavonifractor_plautii (zOTU49*)
s_Eggerthella_lenta
s_Clostridium_scindens
s_Anaerostipes_caccae (zOTU150)
s_Bacteroides_finegoldii
s_Parasutterella_sp000980495
s_Bilophila_wadsworthia (zOTU98)
s_Bacteroides_thetaiotaomicron (zOTU2/66)
s_Bacteroides_faecis
s_Parasutterella_excrementihominis (zOTU42)
s_Enterococcus_gallinarum (zOTU00)
s_Anaerostipes_sp000508985 (zOTU92)
CMc4 CMc34
Ac5 Ac8 Ac20
Bf15 Bf20
P9
-4.8 -3.6 -2.4 -1.2 0.0 1.2 2.4 3.6 4.8
LDA score (log10)
F
Strain found in active mice
MP3
active
inactive
Strain found in inactive mice
Ai7 Ai1
gN4
Er0
Ef11 Ef10 Ef3
CMc21
El8
Fp3
Cb42 Cb30
Rl2
Rg4
s_Clostridium_innocuum (zOTU34*)
g_Niameybacter
s_Thomasclavelia_ramosa (zOTU46*)
s_Clostridium_perfringens
s_Enterococcus_faecalis (zOTU84)
s_Enterocloster_clostridioformis (zOTU5*)
s_Eggerthella_lenta
s_Flavonifractor_plautii (zOTU49*)
s_Enterocloster_bolteae (zOTU5*)
s_Ruthenibacterium_lactatiformans (zOTU78*)
s_Ruminococcus_gnavus (zOTU7)
CPp1
CMc0 CMc50
-4.8 -3.6 -2.4 -1.2 0.0 1.2 2.4 3.6 4.8
LDA score (log10)
G
Species: MP1 MP2 MP3
29
65
28
24
10
11
14
Strain: MP1 MP2 MP3
3
117
70
0
0
2
51
Donor (human)
Ex vivo culture
EEN like
Fiber-rich
Mixture of fermenter samples
Mouse
Active disease
Inactive disease
Mouse diet
chow
EEN-like
Strains/ Species found in mouse
Active
Inactive
shared

Figure 5

532 ***Figure 5: Strains associated with active or inactive disease in Il10$^{-/-}$ mice**:*
533 ***A-C** Transfer overview of donor sample (grey) from FMT 1 (black), FMT 3 (EEN-conditioned, blue) and FMT 4 (FR-*
534 *conditioned, brown) into Il10$^{-/-}$ mice. Mouse inflammation end-points are shown (triangles, red = active, green =*
535 *inactive). Venn diagrams tally strains detected in inflamed (red), non-inflamed (green) Il10$^{-/-}$ mice or found in both*
536 *conditions (yellow) for **A** MP1 **B** MP2 **C** MP3 for each FMT and combined FMT 1, 3 and 4. **D-F** LEfSe (Linear*
537 *discriminant analysis Effect Size) analysis of differentially abundant bacteria at species level based on metagenomic*
538 *data in the recipient inflamed (active, red) or non-inflamed (inactive, green) Il10$^{-/-}$ mice with abundance of strains in*
539 *each condition. Different strains are labeled with different numbers. **D** MP1. **E** MP2. **F** MP3. **G** Venn diagrams shows*
540 *shared or individual species (left) or strains (right) detected in MP1, MP2 and MP3. *zOTUs found in network*
541 *analyses Fig 1G, S2.*

542 **STAR Methods**

543 **RESOURCE AVAILABILITY**

544 **Lead contact**

545 Further information and requests should be directed to and will be fulfilled by the lead contact
546 Prof. Dr. Dirk Haller (dirk.haller@tum.de).

547 **Materials availability**

548 This study did not generate new unique reagents.

549 **Data and code availability**

550 **Data availability**

551 • Some data that support the findings of this study will be available on reasonable request
552 from the corresponding author [TS]. The data are not publicly available due to the
553 pediatric age of the research participants.
554 • Mouse untargeted metabolomics data is available at Massive
555 (https://massive.ucsd.edu) under the number MSV000094047.
556 • 16S rRNA gene sequencing results of the cohort, mouse and fermenter experiments
557 will be available at the time of publication.

558 **Code availability**

559 • Mutliomic data integration of 16S rRNA and metabolomics code is available at
560 https://doi.org/10.5281/zenodo.10808412.
561 • All code necessary to reproduce the metagenomic data analysis will be made publicly
562 available at the time of publication

563

564 **Experimental model and study participant details**

565 **Patient cohort, recruitment and study design**

566 Patients (aged 3-18 years) with suspected or established IBD were recruited to a monocentric
567 pediatric IBD cohort study (ethics approval Ludwig-Maximilians University of Munich, approval
568 No. 17-801 and German Clinical Trials Register Accession No. DRKS00013306, date
569 registration 19.03.2018). All patients and parents/legal guardians provided written informed
570 consent/assent. Patients without confirmed IBD after full diagnostic work-up according to
571 revised Porto criteria were excluded[40]. All other patients were followed prospectively for one

572 year and treated according to current ESPGHAN/ECCO guidelines for CD or ulcerative colitis
573 (UC)/IBD unclassified (IBDU)[6,41,42]. Disease activity, as well as endoscopic, histologic,
574 radiologic and laboratory findings were collected prospectively. Disease activity indices
575 included the Physician Global Assessment (PGA) and the weighted pediatric Crohn's disease
576 activity index (wPCDAI) for CD, as well as the pediatric ulcerative colitis activity index (PUCAI)
577 for UC/IBDU. For EEN-treated CD patients, remission was defined as wPCDAI of <12.5 points
578 and response as reduction in wPCDAI of >17.5 points, but not reaching remission. Relapse
579 was defined as increase of wPCDAI to ≥12.5 points and/or fecal calprotectin of >250 mg/L
580 requiring changes in medical treatment or abdominal surgery or reintroduction of
581 EEN. Patients received detailed instructions for fecal specimen collections and time points, as
582 well as stool collection kits. Each sample was accompanied with a questionnaire on date and
583 time of specimen collection, problems during sampling, Bristol stool scale and recent antibiotic
584 use.

585 EEN therapy was prescribed for 6-8 weeks, followed by gradual re-introduction of solid food
586 and concomitant start of maintenance treatment. EEN was performed with Modulen® IBD
587 (Nestlé Health Science) or in case of intolerance (e.g. cow's milk protein allergy) with Neocate
588 Junior® (Nutricia, Erlangen, Germany). The amount of prescribed formula was based on the
589 Daily Recommendations Intake (DRI) using the online calculator:
590 https://www.nal.usda.gov/human-nutrition-and-food-safety/dri-calculator. All EEN-treated
591 patients received dietary advice and dietetic support to comply with complete liquid formula
592 feeding.

593 **Animal ethics statement**

594 All animal experiments were conducted at Technical University of Munich and approved by the
595 Committee on Animal Health Care and Use of the State of Upper Bavaria (TVA ROB-55.2-
596 2532.Vet_02-19-190) and performed in strict compliance with the EEC recommendations for
597 the care and use of laboratory animals (European Communities Council Directive of November
598 24, 1986 (86/609/EEC).

599 **Animals and housing conditions**

600 GF wild-type (WT) and *Il10*-deficient (*Il10*$^{-/-}$) mice on 129Sv/Ev background were bred and kept
601 at the Core Facility Gnotobiology of the ZIEL Institute for Food & Health, Technical University
602 of Munich, Freising, Germany. Mice were housed as described elsewhere[19], but using single
603 gnoto-cage units (Isocage P System, Tecniplast, Italy). Cages are ventilated with HEPA-
604 filtered air at 22 ± 1°C with a 12-h light/dark cycle. Female and male mice were assigned
605 randomly to the treatment groups with a ratio of 1:1 and six mice per genotype. Mice received
606 standard chow (V1124-300; Ssniff, Soest, Germany; autoclaved) or an EEN-like purified diet
607 (EEN-like, SNIFF S5745-E902, **Fig. S14D**) and sterile water *ad libitum*. EEN-like diet was

608 introduced one week prior to fecal microbial transfer (FMT) to allow for adaptation. Handling
609 of mice in isocages was performed under biological safety cabinets in sterile conditions.

610 Method details

611 Fecal specimen collection

612 Samples were collected at home or in the hospital. Patients provided samples at baseline
613 (before bowel preparation for endoscopy) and every four weeks in (1) 4 mL DNA stabilizer
614 (magiX PBI Microbiome Preservation Buffer, microBIOMix GmbH, Regensburg)[43], (2) 8 mL
615 20% glycerol in reduced phosphate-buffered saline (PBS, 0.05% L-cysteine) and (3) naïve
616 without stabilizing solution. Patients on EEN collected stool in (1) weekly for the first 12 weeks.
617 Samples in (1) were shipped at ambient temperature by mail to the study center. Fecal
618 specimens in (2) and (3) were immediately frozen at home (approx. -18 to -20°C) and brought
619 in on wet ice packs at the next visit. Upon receipt, samples were aliquoted, barcoded, linked
620 to clinical data with CentraXX Bio (Kairos GmbH) and stored immediately at -80°C until further
621 analysis.

622 Selection of donor samples for BONCAT and transfer experiments into germ-free mice

623 We selected Stool samples for direct exposure of MCFAs and FMT experiments into germ-
624 free (GF) mice to show proof-of-concept examples. Therefore, we selected samples based on
625 sampling timepoint (include various states along EEN therapy: active disease sample from
626 treatment-naive patient before the start of EEN (PreEEN, pE), EEN-induced remission (EEN,
627 EE) and a relapse sample after reintroduction of a regular diet (PostEEN, PE)); clinical activity
628 (pga, calprotectin), drug exposure (shorter time under co-medication preferred) and
629 histopathology score in Il10$^{-/-}$ mice of FMT1 (direct transfer). For MP1 (model patient 1) the pE
630 was selected as EE and PE samples induced inflammation in the mouse model, so lowered
631 disease activity in the patient seemed to be influenced by Anit-TNF. PreEEN sample form MP2
632 had very bad quality due to its bloody and diarrhetic consistency, therefore EE and relapse
633 sample were chosen. PE sample in remission was not chosen as a direct impact of EEN
634 therapy was no longer expected. EE sample from MP3 was chosen to investigate a sample
635 where mucosal healing was not fully achieved during EEN therapy. Details are in **Table S3**.

636 Preparing gavage for humanizing germ-free mice

637 Preparation of FMT with human fecal microbiota was performed according to Metwaly *et al*.
638 (2020)[19]. For post *ex vivo* FMT, frozen samples in glycerol (20% end concentration) were
639 thawed on ice. All steps were performed in an anaerobic chamber (90% N_2 and 10% H_2). *Ex*
640 *vivo* suspensions (2 mL) were centrifuged at 100×*g* for 3 min at 4°C to pellet debris.
641 Supernatant was collected and centrifuged at 8000×*g* for 10 min at 4°C to pellet the bacteria.
642 The bacterial pellet was resuspended in 1.5 mL reduced PBS (0.05% L-cysteine-HCl). The

643 clear supernatant was transferred into an anaerobic crimped tube, which was transferred to
644 the gnotobiotic facility. All mice were gavaged on three consecutive days and sacrificed after
645 four weeks of colonization (12 weeks of age).

646 **Tissue Staining and scoring**

647 Colonic and cecal Swiss-roll tissues were fixed, stained and scored as described before[19]. In
648 brief, tissue was fixed in 4% formaldehyde/PBS for 48 h at room temperature, subsequently
649 dehydrated (Leica TP1020), and embedded in paraffin (McCormick; Leica EG1150C).
650 Formalin-fixed paraffin-embedded (FFPE) tissue sections were stained with hematoxylin and
651 eosin (H&E) and scored 0 (not inflamed) to 12 (highly inflamed). Inflammation cut off was
652 defined as a histopathology score greater than three based on scoring in WT mice.

653 **Gene expression**

654 Tissue sections from colon were collected in RNAlater (Sigma Aldrich) for 24 h at 4°C and long-
655 term at -80 °C until processing. Total RNA from tissue was isolated by using the NucleoSpin
656 RNA II kit (Macherey-Nagel GmbH) according to manufacturer's instructions. Complementary
657 DNA was synthetized from 500 ng total RNA by using random hexamers and moloney murine
658 leukemia virus (M-MLV) reverse transcriptase (RT) Point Mutant Synthesis System (Promega).
659 Quantification was performed by using the LightCycler 480 Universal Probe Library System
660 (Roche Primers and probes used were: *Gapdh* (glyceraldehyde 3-phosphate dehydrogenase)
661 (5'-tccactcatggcaaattcaa-3´; 5' tttgatgttagtggggtctcg-3´; Probe #9) and *Tnf* (Tumor necrosis
662 factor) (5´-tgcctatgtctcagcctcttc 3´; 5´-gaggccatttgggaacttct-3´; Probe #49). Relative induction
663 of gene mRNA expression was calculated based the 2-ΔΔCt method [44] using the expression
664 of *Gapdh* for normalization.

665 ***Ex vivo* gut chemostat model**

666 The *ex vivo* continuous fermentation was performed in 1.4-L bioreactors (Multifors 2) and
667 monitored with Eve®software (Infors AG, Basel, Switzerland). Parameters were set as
668 described before[45]. Briefly, vessels were maintained at 37°C, pH 6.8 with a constant influx of
669 N_2 to maintain an anaerobic atmosphere. Inoculation material was prepared in an anaerobic
670 chamber (90% N_2 and 10% H_2). Approximately 2.5 g of frozen fecal samples was suspended
671 in reduced PBS supplemented with 0.03 g/mL L-cysteine-HCl, filtered (70 µm Cell Strainer,
672 FisherScientific) and evenly distributed between two vessels, which led to about 1.0×10^8 to
673 8.16×10^8 CFU/vessel. Two consecutive batch fermentations (24 h in 400 mL, another 24 h
674 with fresh 400 mL medium added) allowed fecal microbial communities to establish.
675 Continuous fermentation included complete medium exchange every 36 h (retention time) with
676 a working volume of 400 mL. After 10 days of continuous fermentation, where stable
677 community formation was achieved, samples for transfer into GF mice were collected and
678 medium was switched afterwards. After 1.5 days of complete medium exchange from medium

679 1 to medium 2, samples for transfer into mice were collected on day 9 of continuous
680 fermentation in the second medium. Medium composition was either fiber-rich (FR) or EEN-
681 like, mimicking patient conditions at sampling (PreEEN and PostEEN, respectively; **Fig. S8A-**
682 **E**).

683 FR medium was prepared according to Macfarlane *et al*. (1998)[46], but supplemented with
684 additional vitamins (pantothenate 10 mg/L, nicotinamide 5 mg/L, thiamine 4 mg/L, biotin 2
685 mg/L, vitamin B12 0.5 mg/L, menadione 1 mg/L, and p-aminobenzoic acid 5 mg/L) as
686 described in Gibson and Wang[47]. EEN-like medium was based on the Macfarlane medium, but
687 with modifications simulating colonic-luminal content during an EEN diet. To determine the
688 carbohydrate:protein ratio of digested Modulen IBD® in the colon, similar calculations as
689 described previously were conducted[48,49]. Since Modulen IBD® lacks fibers, these ingredients
690 present in the FR medium (i.e., pectin from citrus, guar gum, xylan from oat spelt, inulin from
691 *Dahlia* tubers, and arabinogalactan from larch wood) were replaced by soluble rice starch and
692 simple sugars. A total carbohydrate concentration of 13 g/L was chosen in alignment with
693 Cinquin *et al.* (2004)[48]. As the formulation of Modulen IBD® is not publicly available, we
694 decided to include some Modulen IBD® not to miss crucial nutrients in our model-colon
695 medium. Towards this end, 10% of the 1kcal/mL standard preparation of Modulen IBD® was
696 added to 1L of EEN-like medium. Finally, the carbohydrate:protein ratio was 75:25 in the model
697 medium. To further mimic Modulen IBD®, casein was used as main protein source with the
698 exclusion of tryptone and peptone (**Fig. S14A-C**).

699 Samples were aseptically collected daily at the same daytime and stored at -80°C until further
700 analyses. Samples for transfer into the GF mice were collected and mixed with glycerol (20%
701 end concentration) and stored at -80°C until gavage preparation. In order to diminish potential
702 vessel effects in the technical duplicates of each fermenter colonization, samples from both
703 vessels were mixed 50:50 for gavage.

704 **High-throughput 16S-ribosomal RNA (rRNA) gene amplicon sequencing analysis**
705 Total DNA from human stool, colonic mouse content and the continuous *ex vivo* fermentation
706 was isolated using bead beating and sequenced for 16S rRNA gene amplicons as described[50].
707 Downstream analysis was performed in R v4.2.1 using Rhea
708 (https://lagkouvardos.github.io/Rhea/)[51]. zOTU tables were normalized to 10.000 reads, beta-
709 diversity was computed using generalized UniFrac distances[52]. Alpha-diversity was assessed
710 on the basis of taxa richness and Shannon effective number of zOTUs[53]. Trees were visualized
711 and annotated using EvolView (http://www.evolgenius.info/evolview/)[54]. Differential analyses
712 of bacteria in different groups was done using LDA Effect Size (LEfSe)[55]. zOTUs were re-
713 checked using the 16S-based ID tool of EzBioCloud[56] using the database update 2023.08.23,
714 reflecting all taxa published and accepted by IJSEM until April 2023.

715 **Shotgun Metagenomic Sequencing and Analysis**

716 Metagenomic sequencing was performed for 96 human stool samples and 66 samples from
717 transfer experiments (54 mouse, 12 *ex vivo*) using the genomic DNA already isolated for 16S
718 rRNA gene amplicon sequencing. DNA was randomly sheared into short fragments. The
719 obtained fragments were end repaired, A-tailed, and further ligated with Illumina adapters. The
720 fragments with adapters were size-selected, PCR amplified, and purified. The library was
721 checked with Qubit and real-time PCR for quantification and BioAnalyzer for size distribution
722 detection as required by Illumina (TruSeq® DNA Library Prep Kit). Quantified libraries were
723 pooled and sequenced on a NovaSeq platform (Illumina) in PE150 mode. Raw data were
724 aimed at 15 Gb per demultiplexed sample. From raw shotgun metagenomic sequencing data,
725 adapter sequences were removed using Trimmomatic v0.39[57] without considering any
726 mismatch and parameters LEADING:3, TRAILING:3, and SLIDINGWINDOW:4:15. We
727 removed human reads by mapping against human reference genome hg38 by using Bowtie2
728 v2.4.5 [58] with the default parameters. Cleaned fastq data files were used in the following steps.

729 Strain tracking and strain gene content analyses were performed based on the StrainPGC
730 workflow[59]. Briefly, preprocessed metagenomes were metagenotyped using GT-Pro v1.0.1[60].
731 Across all samples, 369 species - as defined in the Unified Human Gut Genome (UHGG)[61] -
732 were robustly detected and only these were included in downstream pangenome profiling.
733 Single nucleotide polymorphism (SNP) profiles were filtered, subsampled, and strain relative
734 abundances were estimated with StrainFacts v0.4.0[18]. Within individual species, estimated
735 strain fractions add up to 100%. By contrast, other analyses considered the overall strain
736 composition: the relative abundance of each strain across all species.

737 Gene profiling was performed against a subset of the MIDASDB-UHGG pangenome database
738 v.15[62] dereplicated at a 99% ANI threshold performed and mapping reads using Bowtie2
739 v2.4.5[58]. Species abundances were estimated based on the average depth of core genes.
740 Global functional gene family profiling was performed by aggregating gene depths into Clusters
741 of Orthologous Genes (COGs) across all species and then normalizing based on 25 ubiquitous,
742 single-copy genes to estimate "gene copies per genome".

743 ***Ex vivo* anaerobic incubations with medium chain fatty acids (MCFAs)**

744 Fecal samples (MP1 PreEEN, MP2 EEN, MP2 relapse, and MP3 EEN) previously collected in
745 20% glycerol in reduced phosphate-buffered saline (PBS, 0.05% L-cysteine) were thawed and
746 introduced into an anaerobic chamber (10% H_2, 90% N_2). All reagents and materials were
747 introduced in the anaerobic chamber 48 hours before sample processing to ensure anaerobic
748 state by the start of the experiment.

749 Stool samples (1-1,5 g) were homogenized with 1X PBS (1:10 dilution) and filtered using a
750 40 µm size filter (Corning, Germany) to remove large particles, which was followed by three

751 washing steps in 1X sterile PBS to remove residual of glycerol and leftover nutrients in the
752 stool. Afterwards, samples were added to sterile falcon tubes containing a final concentration
753 of 50μM of the cellular activity marker L-azidohomoalanine (AHA), (Baseclick GmbH,
754 Germany) and 10μM of MCFAs (lauric acid, decanoid acid and octanoic acid) dissolved in
755 ethanol with a final concentration of 0.5%. 0.5% ethanol was used as negative control and 2
756 mg/mL of glucose as positive control for each experiment. Samples were incubated for 24
757 hours under anaerobic conditions. After 24 hours of incubation, part of the samples were frozen
758 for DNA extraction and other aliquots were washed twice in PBS and then fixed in 1:1
759 ethanol:PBS for further analysis with fluorescence activated cell sorting (FACS). Both ethanol
760 fixed and frozen samples were collected in triplicates[63,64].

761 **Bioorthogonal non-canonical amino acid tagging (BONCAT) and images analysis of**
762 **translationally active bacteria**

763 To identify utilization capability of MCFAs by the gut microbiota, we employed BONCAT, a
764 fluorescence-based single cell labeling technique. BONCAT involves incorporation of the non-
765 canonical amino acid AHA to replace L-methionine during protein synthesis, followed by
766 fluorescent labeling of AHA-containing proteins using azide-alkyne click chemistry[65] (**Fig. 2A**).
767 Cu(I)-catalyzed click chemistry reaction was performed on microscopy slides as previously
768 described[65] and counter-stained with 4′, 6-diamidino-2-phenylindole (DAPI).
769 20 pictures for each sample were collected using a confocal microscope (Olympus, fluoview,
770 FV10i, Germany) and processed using Fiji[66]. Translationally active cells were quantified using
771 the software *digital image analysis in microbial ecology* (Daime)[67]. Translationally active cells
772 were measured as biovolume fraction comparing the Cy5-labeled cells (BONCAT positive) to
773 the total biomass stained with DAPI.

774 **BONCAT-FACS and DNA extraction**

775 A combination of BONCAT and FACS was used to determine which bacteria are capable of
776 MCFAs utilization. Briefly, ethanol fixed samples were washed in 1X sterile PBS, resuspended
777 in 96% ethanol and centrifuged again. Afterwards, the BONCAT dye solution was added to the
778 samples and incubated for 30 min in the dark at room temperature[65]. After incubation, samples
779 were washed three time in 1X sterile PBS and filtered with a 35 mm nylon mesh using BD
780 tubes 12x 75 mm (Corning, Germany) right before sorting. Cy5-positive bacteria were sorted,
781 collected into sterile tubes and store at-80°C until DNA extraction. A representation of the
782 gating strategy is shown in Supplementary Figures 1.
783 Bacterial DNA from sorted and unsorted samples were extracted using the QIAmp DNA mini
784 kit (Qiagen, Germany) following the protocols for bacteria according to the manufacturer's
785 instructions with an additional lysozyme treatment[64]. Every sample was sorted in triplicates.
786 FACS data were further analyzed with FlowJo™ v10.10.0 Software (BD Life Sciences;

787 Reference: FlowJo™ Software (for Windows) Version v10.10.0. Ashland, OR: Becton,
788 Dickinson and Company; 2023).

789 **BONCAT data analysis**

790 Statistical analysis was performed using R statistical software (https://www.r-project.org/). 16S
791 rRNA amplicon sequencing analysis was carried out with Rhea, beta diversity was assessed
792 using UniFrac distances as previously described [51,52] and the statistical significance of factors
793 was evaluated using permutational multivariate analysis of variance (perMANOVA).
794 Differences in relative abundance between sorted and unsorted fractions and between sorted
795 MCFAs and ethanol control, were analyzed using ANOVA and Tukey's test for multiple
796 comparisons. For quantifications of the percentage of active cells, Kruskal-Wallis and Dunn's
797 test were applied. Significantly enriched and depleted zOTUs sequences were identified using
798 the 16S-based ID tool of EzBioCloud[56].

799

800 **Metabolomics**

801 **Sample preparation / Metabolites extraction**

802 **Sample preparation of mouse colon content.** Approximately 20 mg of mouse colon content
803 was weighed in a 2 mL bead beater tube (FastPrep-Tubes, Matrix D, MP Biomedicals Germany
804 GmbH, Eschwege, Germany). Next, 1 mL of methanol-based dehydrocholic acid extraction
805 solvent (c = 1.3 µmol/L) was added as an internal standard for work-up losses. The samples
806 were extracted with a bead beater FastPep-24TM 5G (MP Biomedicals Germany GmbH,
807 Eschwege, Germany) supplied with a CoolPrepTM (MP Biomedicals Germany, cooled with dry
808 ice) 3-times each for 20 s of beating at a speed of 6 m/s and followed by a break of 30 s each.
809 **Sample preparation of fermenter or human samples.** Either 200 mg of the fermenter
810 samples or 100 mg of human fecal samples was weighed in a 15 mL bead beater tube
811 (FastPrep-Tubes, Matrix D, MP Biomedicals Germany GmbH, Eschwege, Germany). Next,
812 5 mL of methanol-based dehydrocholic acid extraction solvent (c = 1.3 µmol/L) was added as
813 an internal standard for work-up losses. The samples were extracted with the same FastPrep
814 protocol described above.
815 **Targeted bile acid measurement.** A standard of 20 µL of isotopically labeled bile acids (ca. 7
816 µM each) were added to 100 µL of sample extract. Targeted bile acid measurement was
817 performed using a QTRAP 5500 triple quadrupole mass spectrometer (Sciex, Darmstadt,
818 Germany) coupled to an ExionLC AD (Sciex, Darmstadt, Germany) ultrahigh performance
819 liquid chromatography system. A multiple reaction monitoring (MRM) method was used for the
820 detection and quantification of the bile acids according to Reiter et. al.[68] Data acquisition and
821 instrumental control were performed with Analyst v1.7 software (Sciex, Darmstadt, Germany).
822 **Untargeted mass spectrometric measurement.** The untargeted analysis was performed
823 using a Nexera UHPLC system (Shimadzu, Duisburg, Germany) coupled to a Q-TOF mass

824 spectrometer (TripleTOF 6600, AB Sciex, Darmstadt, Germany). Separation of the fecal
825 samples was performed either using a UPLC BEH Amide 2.1 × 100 mm, 1.7 µm analytic
826 column (Waters, Eschborn, Germany) with a 400 µL/min flow rate or with a Kinetex XB18 2.1
827 x 100 mm, 1.7 µm (Phenomenex, Aschaffenburg, Germany) with a 300 µL/min flow rate. For
828 the HILIC-separation the settings were as follows: The mobile phase was 5 mM ammonium
829 acetate in water (eluent A) and 5 mM ammonium acetate in acetonitrile/water (95/5, v/v) (eluent
830 B). The gradient profile was 100% B from 0 to 1.5 min, 60% B at 8 min and 20% B at 10 min to
831 11.5 min and 100% B at 12 to 15 min. For the reversed-phase separation, eluent A was 0.1%
832 formic acid and eluent B was 0.1% formic acid in acetonitrile. The gradient profile started with
833 0.2% B which was held for 0.5 min. Afterwards, the concentration of eluent B was increased
834 to 100% until 10 min which was held for 3.25 min. Subsequently, the column was equilibrated
835 at starting conditions. A volume of 5 µL per sample was injected. The autosampler was cooled
836 to 10 °C and the column oven heated to 40 °C. Every tenth run, a quality control (QC) sample,
837 which was pooled from all samples, was injected. The samples were measured in a
838 randomized order and in the Information Dependent Acquisition (IDA) mode. MS settings in
839 the positive mode were as follows: Gas 1 55, Gas 2 65, Curtain gas 35, Temperature 500 °C,
840 Ion Spray Voltage 5500, declustering potential 80. The mass range of the TOF MS and MS/MS
841 scans were 50–2000 m/z and the collision energy was ramped from 15–55 V. MS settings in
842 the negative mode were as follows: Gas 1 55, Gas 2 65, Cur 35, Temperature 500 °C, Ion
843 Spray Voltage -4500, declustering potential -80. The mass range of the TOF MS and MS/MS
844 scans were 50–2000 m/z and the collision energy was ramped from -15–55 V.

845 **Data processing**

846 The "msconvert" from ProteoWizard[69] was used to convert raw files to mzXML (de-noised by
847 centroid peaks). The bioconductor/R package xcms[70] was used for data processing and
848 feature identification. More specifically, the matchedFilter algorithm was used to identify peaks
849 (full width at half-maximum set to 7.5 s). Then the peaks were grouped into features using the
850 "peak density" method[70]. The area under the peak was integrated to represent the abundance
851 of features. The retention time was adjusted based on the peak groups presented in most
852 samples. To annotate features with names of metabolites, the exact mass and MS2
853 fragmentation pattern of the measured features were compared to the records in HMBD[71] and
854 the public MS/MS spectra in MSDIAL[72], referred to as MS1 and MS2 annotation, respectively.
855 Missing values were imputed with half of the limit of detection (LOD) methods, i.e., for every
856 feature, the missing values were replaced with half of the minimal measured value of that
857 feature in all measurements. To confirm a MS2 spectra is well annotated, we manually
858 reviewed our MS2 fragmentation pattern and compared it with records in the public database,
859 previously measured reference standards and SIRIUS[73] to evaluate the correctness of the
860 annotation. Significances of well-annotated metabolic features were computed with analysis

861 of variance (ANOVA) per donor or Wilcoxon signed-rank tests and FDR-corrected using the
862 Benjamin-Hochberg method for three donors. Subsequent hierarchical clustering using only
863 differentially abundant metabolites ($q < 0.05$) was conducted using complete linkage based on
864 Euclidean distances. Calculations, as well as heatmaps, were computed in R v4.2.1. For each
865 principal component analysis (PCA), we included negative and positive features from RP and
866 HILIC with at least 50% non-missing values per condition (inflamed/non-inflamed). The
867 remaining missing values were imputed as described above. The prcomp function from R
868 v4.3.2 computed the principal components after centering and scaling each feature to zero
869 mean and unit variance. Sparse Partial Least Squares Discriminant Analysis (sPLS-DA) was
870 performed on centered and scaled features using the mixOmics bioconductor/R package
871 v6.26.0(Singh et al., 2019). Mean balanced error rate, was used to select the number of
872 components and features in M-fold cross-validation where M corresponds to the minimum
873 number of samples per condition. **Fig. S11** shows raw values for features with the highest
874 Variable Importance in the Projection (VIP), i.e., features contributing the most to explaining
875 the conditions.
876
877 **Data integration of 16s rRNA amplicon data with metabolomics and metagenomics**
878 We matched 60 samples from 15 patients of the 16S-rRNA gene sequencing to 60 samples of
879 the untargeted metabolomics analysis according to patient ID and same time points. The aim
880 was to select features that jointly discriminate the 23 EEN samples (clinical phenotype mild
881 and remission) and 37 PostEEN samples (>2 weeks after EEN, clinical remission). For the
882 integrated selection of metabolome and microbiota features, sPLS-DA (mixOmics v6.20) was
883 used(Singh et al., 2019). For feature selection concerning metabolomics, only annotated
884 metabolites were considered. As described above, input metabolites were mean-centered and
885 scaled to unit variance. zOTUs (zero-radius operational taxonomic units) were centered log-
886 ratio transformed. To estimate the degree of overfitting, the model was trained on 70% of the
887 data, with a k-fold cross-validation for feature selection during training. The remaining 30% of
888 the data were used to evaluate the generalization power. The model performance was
889 measured with an Area Under the Receiver Operating Characteristic (ROC-AUC) on the
890 samples in the test set. Subsequently, Spearman's rank correlation coefficients between all
891 selected metabolites and zOTUs were computed and their respective p-values were corrected
892 with the Benjamini-Hochberg procedure[75]. All coefficients with an FDR >0.05 were set to 0.
893 Using all non-zero correlations, a network was generated and the Louvain method for
894 community detection[76] was applied to extract highly connected subgraphs from the correlation
895 network. For each community, a sPLS-DA model was trained with the same train-test scheme
896 explained previously for feature selection. Using the mean loadings scores over all k iterations,
897 the most relevant metabolites and zOTUs were identified. More precisely, for metabolites and

898 zOTUs separately, the absolute mean loadings were plotted in ascending order and all features
899 on the right of the knee point (20 zOTUs and 22 metabolites) were selected. Analyses were
900 run in R v4.2.1 and python v3.8.11. For network analysis the igraph v1.3.4[77] and networkx
901 v3.1[78] packages were used.

902 Profiles of 16S rRNA amplicon relative abundance were further integrated with metagenomic
903 species profiles in order to identify those which represent the same, underlying taxa. This was
904 done by cross-decomposition of zOTU relative abundance and species relative abundances
905 estimated from the metagenomic workflow, using the PLSSVD model implemented in SciKit-
906 Learn[79], multiplying the matrices of weights for each data-type provides a matrix of coefficients
907 mapping zOTUs to metagenomic species. We scaled these coefficients by the square-root of
908 the mean relative abundance of that zOTU and species, respectively, producing a matrix of
909 matching scores for each comparison, while accounting for all other taxa. Based on this score,
910 we ranked zOTUs for each species and species for each zOTU. We selected as putative
911 matches all zOTU-species pairs that were either reciprocal best hits or a combination of one
912 best hit and one second-best hit, and where at least one of the genus or family classifications
913 matched. In this way, we accounted for the possibility of multiple zOTUs representing a species
914 or multiple species being represented by a zOTU.

915 **Statistical analysis**

916 MDS and PCA latent dimensions in **Fig. 1** and **Fig. S1** were tested for significance using linear
917 mixed models of the form

918 $$\text{axis} \sim \text{intercept} + \text{diet} + \text{disease} + \text{diet} * \text{disease} + (1|\text{patient})$$

919 where diet, disease and their interaction are included as fixed effects and patients are included
920 as random effects. All coefficients are tested with a t-test for **Fig. 1** and an ANOVA for **Fig. S1**.
921 Reported p-values are Bonferroni-corrected. To estimate the degrees of freedom, we used
922 Satterthwaite's method as implemented in the lmerTest package (version 3.1-3).
923 Further statistical analyses and plots were generated using GraphPad Prism v8.0 (GraphPad,
924 La Jolla, CA) using Mann-Whitney test, ANOVA followed by pairwise comparison testing
925 (Tukey, Bonferroni correction), by Kruskal-Wallis test followed by Dunn`s multiple comparisons.
926 Data is presented as mean ± SD. P-values below 0.05 were considered significant ($p < 0.05$,
927 *; $p < 0.01$, **; $p < 0.001$, ***; and $p < 0.0001$, ****).

928 Taxonomic turnover in both zOTU and strain compositions were calculated based on the Bray-
929 Curtis dissimilarity. Pairs where one sample was collected during EEN and the other during
930 PostEEN were classified as “transition”. All within-subject pairwise comparisons were
931 computed and fit using cubic spline regression of the time between sample collections, with a

932 regression term for each subject, as well as for each pair class: EEN, transition, or PostEEN.
933 The null hypothesis of no difference between pair classes was tested by permutation: 999
934 random permutations of samples within subjects. Changes in mean, normalized, COG depths
935 during EEN and PostEEN time points were tested using the Wilcoxon signed-rank test across
936 subjects. False discovery rates were calculated using the Benjamini-Hochberg procedure.
937 Mean fold change for each COG was calculated as the ratio between these two estimates.

938 Additional resources

939 Clinical Trial Registry

940 The study is registered at the German Clinical Trials Registry under the Accession No.
941 DRKS00013306, date of registration 19.03.2018.

Supplementary Data

Supplemental information.

Document S1. Figures S1-S14, Tables S1-S5:

Figures S1-S3 related to Figure 1.
Tables S1- S2 related to Figure 1.
Table S3 related to donor sample selection related to Figure 2 -5
Figures S4-S5 and tables S4-S5 related to Figure 2
Figures S6 and tables S6 and S7 are related to Figure 3.
Figures S7-S8 related to Figure 4.
Figures S9-S13 related to Figure 5.
Figures S14 related to media and diet information in STARMethods.

Tables S6 and S7: Excel files containing additional data too large to fit in a PDF. Related to Figure 3.

References

1. Torres, J., Mehandru, S., Colombel, J.F., and Peyrin-Biroulet, L. (2017). Crohn's disease. Lancet *389*, 1741–1755. https://doi.org/10.1016/S0140-6736(16)31711-1.

2. Kuenzig, M.E., Fung, S.G., Marderfeld, L., Mak, J.W.Y., Kaplan, G.G., Ng, S.C., Wilson, D.C., Cameron, F., Henderson, P., Kotze, P.G., et al. (2022). Twenty-first Century Trends in the Global Epidemiology of Pediatric-Onset Inflammatory Bowel Disease: Systematic Review. Gastroenterology *162*, 1147-1159.e4. https://doi.org/10.1053/j.gastro.2021.12.282.

3. Kaplan, G.G., and Ng, S.C. (2017). Understanding and Preventing the Global Increase of Inflammatory Bowel Disease. Gastroenterology *152*, 313-321.e2. https://doi.org/10.1053/j.gastro.2016.10.020.

4. Liu, Z., Liu, R., Gao, H., Jung, S., Gao, X., Sun, R., Liu, X., Kim, Y., Lee, H.S., Kawai, Y., et al. (2023). Genetic architecture of the inflammatory bowel diseases across East Asian and European ancestries. Nat Genet *55*, 796. https://doi.org/10.1038/S41588-023-01384-0.

5. Renz, H., Von Mutius, E., Brandtzaeg, P., Cookson, W.O., Autenrieth, I.B., and Haller, D. (2011). Gene-environment interactions in chronic inflammatory disease. Nature Immunology 2011 12:4 *12*, 273–277. https://doi.org/10.1038/ni0411-273.

6. Van Rheenen, P.F., Aloi, M., Assa, A., Bronsky, J., Escher, J.C., Fagerberg, U.L., Gasparetto, M., Gerasimidis, K., Griffiths, A., Henderson, P., et al. (2020). The Medical Management of Paediatric Crohn's Disease: an ECCO-ESPGHAN Guideline Update. J Crohns Colitis *15*, 171–194. https://doi.org/10.1093/ECCO-JCC/JJAA161.

7. Agrawal, M., Spencer, E.A., Colombel, J.-F., and Ungaro, R.C. (2021). Approach to the Management of Recently Diagnosed Inflammatory Bowel Disease Patients: A User's Guide for Adult and Pediatric Gastroenterologists. Gastroenterology *161*, 47–65. https://doi.org/10.1053/j.gastro.2021.04.063.

8. Bischoff, S.C., Bager, P., Escher, J., Forbes, A., Hébuterne, X., Hvas, C.L., Joly, F., Klek, S., Krznaric, Z., Ockenga, J., et al. (2023). ESPEN guideline on Clinical Nutrition in inflammatory bowel disease. Clinical Nutrition *42*, 352–379. https://doi.org/10.1016/j.clnu.2022.12.004.

9. Logan, M., Gkikas, K., Svolos, V., Nichols, B., Milling, S., Gaya, D.R., Seenan, J.P., Macdonald, J., Hansen, R., Ijaz, U.Z., et al. (2020). Analysis of 61 exclusive enteral nutrition formulas used in the management of active Crohn's disease—new insights into dietary disease triggers. Aliment Pharmacol Ther *51*, 935–947. https://doi.org/10.1111/APT.15695.

10. Logan, M., Clark, C.M., Ijaz, U.Z., Gervais, L., Duncan, H., Garrick, V., Curtis, L., Buchanan, E., Cardigan, T., Armstrong, L., et al. (2019). The reduction of faecal calprotectin during exclusive enteral nutrition is lost rapidly after food re-introduction. Aliment Pharmacol Ther *50*, 664. https://doi.org/10.1111/APT.15425.

11. Schwerd, T., Frivolt, K., Clavel, T., Lagkouvardos, I., Katona, G., Mayr, D., Uhlig, H.H., Haller, D., Koletzko, S., and Bufler, P. (2016). Exclusive enteral nutrition in active pediatric Crohn disease: Effects on intestinal microbiota and immune regulation. Journal

of Allergy and Clinical Immunology *138*, 592–596. https://doi.org/10.1016/j.jaci.2015.12.1331.

12. Frivolt, K., Schwerd, T., Werkstetter, K.J., Schwarzer, A., Schatz, S.B., Bufler, P., and Koletzko, S. (2014). Repeated exclusive enteral nutrition in the treatment of paediatric Crohn's disease: Predictors of efficacy and outcome. Aliment Pharmacol Ther *39*, 1398–1407. https://doi.org/10.1111/apt.12770.

13. Metwaly, A., Reitmeier, S., and Haller, D. (2022). Microbiome risk profiles as biomarkers for inflammatory and metabolic disorders. Nature Reviews Gastroenterology & Hepatology 2022 19:6 *19*, 383–397. https://doi.org/10.1038/s41575-022-00581-2.

14. Schirmer, M., Garner, A., Vlamakis, H., and Xavier, R.J. (2019). Microbial genes and pathways in inflammatory bowel disease. Nat Rev Microbiol *17*, 497. https://doi.org/10.1038/S41579-019-0213-6.

15. Lavelle, A., and Sokol, H. (2020). Gut microbiota-derived metabolites as key actors in inflammatory bowel disease. Nature Reviews Gastroenterology & Hepatology 2020 17:4 *17*, 223–237. https://doi.org/10.1038/s41575-019-0258-z.

16. Pereira, G.V., Boudaud, M., Wolter, M., Alexander, C., De Sciscio, A., Grant, E.T., Trindade, B.C., Pudlo, N.A., Singh, S., Campbell, A., et al. (2024). Opposing diet, microbiome, and metabolite mechanisms regulate inflammatory bowel disease in a genetically susceptible host. Cell Host Microbe *32*, 527-542.e9. https://doi.org/10.1016/j.chom.2024.03.001.

17. Tanes, C., Bittinger, K., Gao, Y., Friedman, E.S., Nessel, L., Paladhi, U.R., Chau, L., Panfen, E., Fischbach, M.A., Braun, J., et al. (2021). Role of dietary fiber in the recovery of the human gut microbiome and its metabolome. Cell Host Microbe *29*, 394-407.e5. https://doi.org/10.1016/j.chom.2020.12.012.

18. Smith, B.J., Li, X., Shi, Z.J., Abate, A., and Pollard, K.S. (2022). Scalable Microbial Strain Inference in Metagenomic Data Using StrainFacts. Frontiers in Bioinformatics *2*. https://doi.org/10.3389/fbinf.2022.867386.

19. Metwaly, A., Dunkel, A., Waldschmitt, N., Raj, A.C.D., Lagkouvardos, I., Corraliza, A.M., Mayorgas, A., Martinez-Medina, M., Reiter, S., Schloter, M., et al. (2020). Integrated microbiota and metabolite profiles link Crohn's disease to sulfur metabolism. Nature Communications 2020 11:1 *11*, 1–15. https://doi.org/10.1038/s41467-020-17956-1.

20. Jiang, J., Chen, L., Chen, Y., and Chen, H. (2022). Exclusive enteral nutrition remodels the intestinal flora in patients with active Crohn's disease. BMC Gastroenterol *22*. https://doi.org/10.1186/S12876-022-02293-Y.

21. Vich Vila, A., Imhann, F., Collij, V., Jankipersadsing, S.A., Gurry, T., Mujagic, Z., Kurilshikov, A., Bonder, M.J., Jiang, X., Tigchelaar, E.F., et al. (2018). Gut microbiota composition and functional changes in inflammatory bowel disease and irritable bowel syndrome. Sci Transl Med *10*. https://doi.org/10.1126/scitranslmed.aap8914.

22. Podlesny, D., Durdevic, M., Paramsothy, S., Kaakoush, N.O., Högenauer, C., Gorkiewicz, G., Walter, J., and Fricke, W.F. (2022). Identification of clinical and ecological determinants of strain engraftment after fecal microbiota transplantation using metagenomics. Cell Rep Med *3*, 100711. https://doi.org/10.1016/j.xcrm.2022.100711.

1041 23. Yang, H.T., Chen, J.W., Rathod, J., Jiang, Y.Z., Tsai, P.J., Hung, Y.P., Ko, W.C., Paredes-
1042 Sabja, D., and Huang, I.H. (2018). Lauric acid is an inhibitor of Clostridium difficile
1043 growth in vitro and reduces inflammation in a mouse infection model. Front Microbiol *8*,
1044 2635. https://doi.org/10.3389/FMICB.2017.02635/FULL.

1045 24. Kabara, J.J., Swieczkowski, D.M., Conley, A.J., and Truant, J.P. (1972). Fatty acids and
1046 derivatives as antimicrobial agents. Antimicrob Agents Chemother *2*, 23–28.
1047 https://doi.org/10.1128/AAC.2.1.23.

1048 25. Huang, W.C., Tsai, T.H., Chuang, L. Te, Li, Y.Y., Zouboulis, C.C., and Tsai, P.J. (2014).
1049 Anti-bacterial and anti-inflammatory properties of capric acid against Propionibacterium
1050 acnes: A comparative study with lauric acid. J Dermatol Sci *73*, 232–240.
1051 https://doi.org/10.1016/j.jdermsci.2013.10.010.

1052 26. Sorrentino, G., Perino, A., Yildiz, E., El Alam, G., Bou Sleiman, M., Gioiello, A.,
1053 Pellicciari, R., and Schoonjans, K. (2020). Bile Acids Signal via TGR5 to Activate
1054 Intestinal Stem Cells and Epithelial Regeneration. Gastroenterology *159*, 956-968.e8.
1055 https://doi.org/10.1053/j.gastro.2020.05.067.

1056 27. Xiao, F., Gao, X., Hu, H., Le, J., Chen, Y., Shu, X., Liang, Z., Xu, Y., Wang, Y., and Zhang,
1057 T. (2022). Exclusive Enteral Nutrition Exerts Anti-Inflammatory Effects through
1058 Modulating Microbiota, Bile Acid Metabolism, and Immune Activities. Nutrients *14*, 4463.
1059 https://doi.org/10.3390/NU14214463/S1.

1060 28. Lv, Y., Lou, Y., Liu, A., Cheng, Q., Yang, G., Xu, C., Luo, Y., Lou, J., Yu, J., Fang, Y., et
1061 al. (2023). The impact of exclusive enteral nutrition on the gut microbiome and bile acid
1062 metabolism in pediatric Crohn's disease. Clinical Nutrition *42*, 116–128.
1063 https://doi.org/10.1016/j.clnu.2022.11.018.

1064 29. Gill, S.K., Rossi, M., Bajka, B., and Whelan, K. (2020). Dietary fibre in gastrointestinal
1065 health and disease. Nature Reviews Gastroenterology & Hepatology 2020 18:2 *18*,
1066 101–116. https://doi.org/10.1038/s41575-020-00375-4.

1067 30. Schroeder, B.O., Birchenough, G.M.H., Ståhlman, M., Arike, L., Johansson, M.E.V.,
1068 Hansson, G.C., and Bäckhed, F. (2018). Bifidobacteria or Fiber Protects against Diet-
1069 Induced Microbiota-Mediated Colonic Mucus Deterioration. Cell Host Microbe *23*, 27-
1070 40.e7. https://doi.org/10.1016/j.chom.2017.11.004.

1071 31. Desai, M.S., Seekatz, A.M., Koropatkin, N.M., Kamada, N., Hickey, C.A., Wolter, M.,
1072 Pudlo, N.A., Kitamoto, S., Terrapon, N., Muller, A., et al. (2016). A Dietary Fiber-Deprived
1073 Gut Microbiota Degrades the Colonic Mucus Barrier and Enhances Pathogen
1074 Susceptibility. Cell *167*, 1339-1353.e21. https://doi.org/10.1016/j.cell.2016.10.043.

1075 32. Haskey, N., Gold, S.L., Faith, J.J., and Raman, M. (2023). To Fiber or Not to Fiber: The
1076 Swinging Pendulum of Fiber Supplementation in Patients with Inflammatory Bowel
1077 Disease. Nutrients 2023, Vol. 15, Page 1080 *15*, 1080.
1078 https://doi.org/10.3390/NU15051080.

1079 33. Armstrong, H., Mander, I., Zhang, Z., Armstrong, D., and Wine, E. (2021). Not All Fibers
1080 Are Born Equal; Variable Response to Dietary Fiber Subtypes in IBD. Front Pediatr *8*,
1081 620189. https://doi.org/10.3389/fped.2020.620189.

1082 34. Armstrong, H.K., Bording-Jorgensen, M., Santer, D.M., Zhang, Z., Valcheva, R., Rieger,
1083 A.M., Sung-Ho Kim, J., Dijk, S.I., Mahmood, R., Ogungbola, O., et al. (2023).

Unfermented β-fructan Fibers Fuel Inflammation in Select Inflammatory Bowel Disease Patients. Gastroenterology *164*, 228–240. https://doi.org/10.1053/j.gastro.2022.09.034.

35. Arifuzzaman, M., Won, T.H., Li, T.T., Yano, H., Digumarthi, S., Heras, A.F., Zhang, W., Parkhurst, C.N., Kashyap, S., Jin, W.B., et al. (2022). Inulin fibre promotes microbiota-derived bile acids and type 2 inflammation. Nature 2022 611:7936 *611*, 578–584. https://doi.org/10.1038/s41586-022-05380-y.

36. Singh, V., Yeoh, B.S., Walker, R.E., Xiao, X., Saha, P., Golonka, R.M., Cai, J., Bretin, A.C.A., Cheng, X., Liu, Q., et al. (2019). Microbiota fermentation-NLRP3 axis shapes the impact of dietary fibres on intestinal inflammation. Gut *68*, 1801–1812. https://doi.org/10.1136/GUTJNL-2018-316250.

37. Kuffa, P., Pickard, J.M., Campbell, A., Yamashita, M., Schaus, S.R., Martens, E.C., Schmidt, T.M., Inohara, N., Núñez, G., and Caruso, R. (2023). Fiber-deficient diet inhibits colitis through the regulation of the niche and metabolism of a gut pathobiont. Cell Host Microbe. https://doi.org/10.1016/J.CHOM.2023.10.016.

38. Metwaly, A., Jovic, J., Waldschmitt, N., Khaloian, S., Heimes, H., Häcker, D., Ahmed, M., Hammoudi, N., Le Bourhis, L., Mayorgas, A., et al. (2023). Diet prevents the expansion of segmented filamentous bacteria and ileo-colonic inflammation in a model of Crohn's disease. Microbiome *11*, 66. https://doi.org/10.1186/s40168-023-01508-y.

39. Turner, D., Ricciuto, A., Lewis, A., D'Amico, F., Dhaliwal, J., Griffiths, A.M., Bettenworth, D., Sandborn, W.J., Sands, B.E., Reinisch, W., et al. (2021). STRIDE-II: An Update on the Selecting Therapeutic Targets in Inflammatory Bowel Disease (STRIDE) Initiative of the International Organization for the Study of IBD (IOIBD): Determining Therapeutic Goals for Treat-to-Target strategies in IBD. Gastroenterology *160*, 1570–1583. https://doi.org/10.1053/J.GASTRO.2020.12.031.

40. Levine, A., Koletzko, S., Turner, D., Escher, J.C., Cucchiara, S., de Ridder, L., Kolho, K.-L., Veres, G., Russell, R.K., Paerregaard, A., et al. (2014). ESPGHAN Revised Porto Criteria for the Diagnosis of Inflammatory Bowel Disease in Children and Adolescents. J Pediatr Gastroenterol Nutr *58*, 795–806. https://doi.org/10.1097/MPG.0000000000000239.

41. Turner, D., Ruemmele, F.M., Orlanski-Meyer, E., Griffiths, A.M., De Carpi, J.M., Bronsky, J., Veres, G., Aloi, M., Strisciuglio, C., Braegger, C.P., et al. (2018). Management of paediatric ulcerative colitis, part 1: Ambulatory Care-An Evidence-based Guideline From European Crohn's and Colitis Organization and European Society of Paediatric Gastroenterology, Hepatology and Nutrition. J Pediatr Gastroenterol Nutr *67*, 257–291. https://doi.org/10.1097/MPG.0000000000002035.

42. Turner, D., Ruemmele, F.M., Orlanski-Meyer, E., Griffiths, A.M., De Carpi, J.M., Bronsky, J., Veres, G., Aloi, M., Strisciuglio, C., Braegger, C.P., et al. (2018). Management of paediatric ulcerative colitis, part 2: Acute severe colitis - An evidence-based consensus guideline from the european Crohn's and colitis organization and the european society of paediatric gastroenterology, hepatology and nutrition. J Pediatr Gastroenterol Nutr *67*, 292–310. https://doi.org/10.1097/MPG.0000000000002036.

43. Schult, D., Reitmeier, S., Koyumdzhieva, P., Lahmer, T., Middelhof, M., Erber, J., Schneider, J., Kager, J., Frolova, M., Horstmann, J., et al. (2022). Gut bacterial dysbiosis

and instability is associated with the onset of complications and mortality in COVID-19. Gut Microbes *14*. https://doi.org/10.1080/19490976.2022.2031840.

44. Livak, K.J., and Schmittgen, T.D. (2001). Analysis of Relative Gene Expression Data Using Real-Time Quantitative PCR and the 2−ΔΔCT Method. Methods *25*, 402–408. https://doi.org/10.1006/METH.2001.1262.

45. Püngel, D., Treveil, A., Dalby, M.J., Caim, S., Colquhoun, I.J., Booth, C., Ketskemety, J., Korcsmaros, T., van Sinderen, D., Lawson, M.A., et al. (2020). Bifidobacterium breve UCC2003 Exopolysaccharide Modulates the Early Life Microbiota by Acting as a Potential Dietary Substrate. Nutrients *12*, 948. https://doi.org/10.3390/nu12040948.

46. Macfarlane, G.T., Macfarlane, S., and Gibson, G.R. (1998). Validation of a three-stage compound continuous culture system for investigating the effect of retention time on the ecology and metabolism of bacteria in the human colon. Microb Ecol *35*, 180–187. https://doi.org/10.1007/s002489900072.

47. Gibson, G.R., and Wang, X. (1994). Enrichment of bifidobacteria from human gut contents by oligofructose using continuous culture. FEMS Microbiol Lett *118*, 121–127. https://doi.org/10.1016/0378-1097(94)90606-8.

48. Cinquin, C., Le Blay, G., Fliss, I., and Lacroix, C. (2004). Immobilization of infant fecal microbiota and utilization in an in vitro colonic fermentation model. Microb Ecol *48*, 128–138. https://doi.org/10.1007/s00248-003-2022-7.

49. Poeker, S.A., Lacroix, C., de Wouters, T., Spalinger, M.R., Scharl, M., and Geirnaert, A. (2019). Stepwise Development of an in vitro Continuous Fermentation Model for the Murine Caecal Microbiota. Front Microbiol *10*. https://doi.org/10.3389/fmicb.2019.01166.

50. Reitmeier, S., Kiessling, S., Neuhaus, K., and Haller, D. (2020). Comparing Circadian Rhythmicity in the Human Gut Microbiome. STAR Protoc *1*, 100148. https://doi.org/10.1016/j.xpro.2020.100148.

51. Lagkouvardos, I., Fischer, S., Kumar, N., and Clavel, T. (2017). Rhea: a transparent and modular R pipeline for microbial profiling based on 16S rRNA gene amplicons. PeerJ *5*, e2836. https://doi.org/10.7717/peerj.2836.

52. Chen, J., Bittinger, K., Charlson, E.S., Hoffmann, C., Lewis, J., Wu, G.D., Collman, R.G., Bushman, F.D., and Li, H. (2012). Associating microbiome composition with environmental covariates using generalized UniFrac distances. Bioinformatics *28*, 2106–2113. https://doi.org/10.1093/bioinformatics/bts342.

53. Jost, L. (2007). Partitioning diversity into independent alpha and beta components. Ecology *88*, 2427–2439. https://doi.org/10.1890/06-1736.1.

54. Subramanian, B., Gao, S., Lercher, M.J., Hu, S., and Chen, W.H. (2019). Evolview v3: a webserver for visualization, annotation, and management of phylogenetic trees. Nucleic Acids Res *47*, W270–W275. https://doi.org/10.1093/NAR/GKZ357.

55. Segata, N., Izard, J., Waldron, L., Gevers, D., Miropolsky, L., Garrett, W.S., and Huttenhower, C. (2011). Metagenomic biomarker discovery and explanation. Genome Biol *12*, R60. https://doi.org/10.1186/GB-2011-12-6-R60.

56. Yoon, S.-H., Ha, S.-M., Kwon, S., Lim, J., Kim, Y., Seo, H., and Chun, J. (2017). Introducing EzBioCloud: a taxonomically united database of 16S rRNA gene sequences and whole-genome assemblies. Int J Syst Evol Microbiol *67*, 1613–1617. https://doi.org/10.1099/ijsem.0.001755.

57. Bolger, A.M., Lohse, M., and Usadel, B. (2014). Trimmomatic: a flexible trimmer for Illumina sequence data. Bioinformatics *30*, 2114–2120. https://doi.org/10.1093/BIOINFORMATICS/BTU170.

58. Langmead, B., and Salzberg, S.L. (2012). Fast gapped-read alignment with Bowtie 2. Nature Methods 2012 9:4 *9*, 357–359. https://doi.org/10.1038/nmeth.1923.

59. Smith, B.J., Zhao, C., Dubinkina, V., Jin, X., Moltzau-Anderson, J., Pollard, K.S., Biohub, C.Z., and Francisco, S. (2024). Accurate estimation of intraspecific microbial gene content variation in metagenomic data with MIDAS v3 and StrainPGC. bioRxiv, 2024.04.10.588779. https://doi.org/10.1101/2024.04.10.588779.

60. Shi, Z.J., Dimitrov, B., Zhao, C., Nayfach, S., and Pollard, K.S. (2021). Fast and accurate metagenotyping of the human gut microbiome with GT-Pro. Nature Biotechnology 2021 40:4 *40*, 507–516. https://doi.org/10.1038/s41587-021-01102-3.

61. Almeida, A., Nayfach, S., Boland, M., Strozzi, F., Beracochea, M., Shi, Z.J., Pollard, K.S., Sakharova, E., Parks, D.H., Hugenholtz, P., et al. (2020). A unified catalog of 204,938 reference genomes from the human gut microbiome. Nature Biotechnology 2020 39:1 *39*, 105–114. https://doi.org/10.1038/s41587-020-0603-3.

62. Zhao, C., Dimitrov, B., Goldman, M., Nayfach, S., and Pollard, K.S. (2023). MIDAS2: Metagenomic Intra-species Diversity Analysis System. Bioinformatics *39*. https://doi.org/10.1093/BIOINFORMATICS/BTAC713.

63. Deehan, E.C., Zhang, Z., Riva, A., Armet, A.M., Perez-Muñoz, M.E., Nguyen, N.K., Krysa, J.A., Seethaler, B., Zhao, Y.-Y., Cole, J., et al. (2022). Elucidating the role of the gut microbiota in the physiological effects of dietary fiber. Microbiome *10*, 77. https://doi.org/10.1186/s40168-022-01248-5.

64. Riva, A., Rasoulimehrabani, H., Cruz-Rubio, J.M., Schnorr, S.L., von Baeckmann, C., Inan, D., Nikolov, G., Herbold, C.W., Hausmann, B., Pjevac, P., et al. (2023). Identification of inulin-responsive bacteria in the gut microbiota via multi-modal activity-based sorting. Nature Communications 2023 14:1 *14*, 1–15. https://doi.org/10.1038/s41467-023-43448-z.

65. Hatzenpichler, R., Scheller, S., Tavormina, P.L., Babin, B.M., Tirrell, D.A., and Orphan, V.J. (2014). <scp> *In situ* </scp> visualization of newly synthesized proteins in environmental microbes using amino acid tagging and click chemistry. Environ Microbiol *16*, 2568–2590. https://doi.org/10.1111/1462-2920.12436.

66. Schindelin, J., Arganda-Carreras, I., Frise, E., Kaynig, V., Longair, M., Pietzsch, T., Preibisch, S., Rueden, C., Saalfeld, S., Schmid, B., et al. (2012). Fiji: an open-source platform for biological-image analysis. Nature Methods 2012 9:7 *9*, 676–682. https://doi.org/10.1038/nmeth.2019.

67. Daims, H., Lücker, S., and Wagner, M. (2006). daime, a novel image analysis program for microbial ecology and biofilm research. Environ Microbiol *8*, 200–213. https://doi.org/10.1111/J.1462-2920.2005.00880.X.